

1 **Scaling regimes and linear / nonlinear responses of last** 2 **millennium climate to volcanic and solar forcings**

3 S. Lovejoy¹, and C. Varotsos²

4 ¹Physics, McGill University, 3600 University St., Montreal, Que., Canada

5 ²Climate Research Group, Division of Environmental Physics and Meteorology, Faculty of Physics, University of Athens,
6 University Campus Bldg. Phys. V, Athens 15784, Greece

7 Correspondence to: S. Lovejoy (lovejoy@physics.mcgill.ca) and C. Varotsos (covar@phys.uoa.gr)

8 **Abstract.** At scales much longer than the deterministic predictability limits (about 10 days), the statistics of the atmosphere
9 undergoes a drastic transition, the high frequency weather acts as a random forcing on the lower frequency macroweather. In
10 addition, up to decadal and centennial scales the equivalent radiative forcings of solar, volcanic and anthropogenic perturbations
11 are small compared to the mean incoming solar flux. This justifies the common practice of reducing forcings to radiative
12 equivalents (which are assumed to combine linearly), as well as the development of linear stochastic models, including for
13 forecasting at monthly to decadal scales.

14 In order to clarify the validity of the linearity assumption and determine its scale range, we use last Millennium simulations, both
15 with the simplified Zebiac- Cane (ZC) model and the NASA GISS E2-R fully coupled GCM. We systematically compare the
16 statistical properties of solar only, volcanic only and combined solar and volcanic forcings over the range of time scales from one
17 to 1000 years. We also compare the statistics to multiproxy temperature reconstructions. The main findings are: a) that the
18 variability of the ZC and GCM models are too weak at centennial and longer scales, b) for longer than ≈ 50 years, the solar and
19 volcanic forcings combine subadditively (nonlinearly) compounding the weakness of the response, c) the models display another
20 nonlinear effect at shorter scales: their sensitivities are much higher for weak forcing than for strong forcing (their intermittencies
21 are different) and we quantify this with statistical scaling exponents.

22 **1. Introduction**

23 **1.1 Linearity versus nonlinearity**

24 The GCM approach to climate modeling is based on the idea that whereas weather is an initial value problem, the climate is a
25 boundary value problem (Bryson, 1997; Pielke, 1998). This means that although the weather's sensitive dependence on initial
26 conditions (chaos, the "butterfly effect") leads to a loss of predictability at time scales of about 10 days, nevertheless averaging
27 over enough "weather" leads to a convergence to the model's "climate". This climate is thus the state to which averages of model
28 outputs converge for fixed atmospheric compositions and boundary conditions (i.e. control runs).

29 The question then arises as to the response of the system to small changes in the boundary conditions: for example
30 anthropogenic forcings are less than 2 W/m^2 , and at least over scales of several years, solar and volcanic forcings are of similar
31 magnitude or smaller (see e.g. Fig. 1a and the quantification in Fig. 2). These numbers are of the order of 1% of the mean solar
32 radiative flux so that we may anticipate that the atmosphere responds fairly linearly. This is indeed that usual assumption and it
33 justifies the reduction of potentially complex forcings to overall radiative forcings (see Meehl et al., 2004) for GCM

34 investigations at annual scales and Hansen et al., (2005) for Greenhouse gases. However, at long enough scales, linearity
 35 clearly breaks down, indeed starting with the celebrated “Daisy world” model (Watson and Lovelock, 1983), there is a whole
 36 literature that uses energy balance models to study the strongly nonlinear interactions/feedbacks between global temperatures
 37 and albedoes. There is no debate that temperature-albedo feedbacks are important at the multimillennial scales of the glacial-
 38 interglacial transitions. While some authors (e.g. Roques et al., 2014) use time scales as short as 200 years for the critical ice-
 39 albedo feedbacks, others have assumed that the temperature response to solar and volcanic forcings over the last millennium are
 40 reasonably linear (e.g. Østvand et al., 2014; Rypdal and Rypdal, 2014) while Pelletier, (1998) and Fraedrich et al., (2009) assume
 41 linearity to even longer scales.

42 It is therefore important to establish the times scales over which linear responses are a reasonable assumption. However,
 43 clearly even over scales where typical responses to small forcings are relatively linear, the response may be nonlinear if the
 44 forcing is – volcanic or volcanic- like i.e. if it is sufficiently “spikey” or intermittent.

45 1.2 Atmospheric variability: scaling regimes

46 Before turning our attention to models, what can we learn empirically? Certainly, at high enough frequencies (the weather
 47 regime), the atmosphere is highly nonlinear. However, at about ten days, the atmosphere undergoes a drastic transition to a lower
 48 frequency regime, and this “macroweather” regime is potentially quasi- linear in its responses. Indeed, the basic atmospheric
 49 scaling regimes were identified some time ago - primarily using spectral analysis (Lovejoy and Schertzer, 1986; Pelletier, 1998;
 50 Shackleton and Imbrie, 1990; Huybers and Curry, 2006). However, the use of real space fluctuations provided a clearer picture
 51 and a simpler interpretation. It also showed that the usual view of atmospheric variability, as a sequence of narrow scale range
 52 processes (e.g. nonlinear oscillators), has seriously neglected the main source of variability, namely the scaling “background
 53 spectrum” (Lovejoy, 2014). What was found is that for virtually all atmospheric fields, there was a transition from the behavior
 54 of the mean temperature fluctuations scaling $\langle \Delta T(\Delta t) \rangle \approx \Delta t^H$ with $H > 0$ to a lower frequency scaling regime with $H < 0$ at
 55 scales $\Delta t \gtrsim 10$ days; the macroweather regime. The transition scale of around 10 days, can be theoretically predicted on the
 56 basis of the scaling of the turbulent wind due to solar forcing (via the imposed energy rate density; see (Lovejoy and Schertzer,
 57 2010; Lovejoy and Schertzer, 2013; Lovejoy et al., 2014). Whereas the weather is naturally identified with the high frequency
 58 $H > 0$ regime and with temperature values “wandering” up and down like a drunkard’s walk, the lower frequency $H < 0$
 59 regime is characterized by fluctuations tending to cancel out – effectively starting to converge. This converging regime is a low
 60 frequency type of weather, described as “macroweather” (Lovejoy, 2013; Lovejoy et al., 2014). For the GCM control runs,
 61 macroweather effectively continues to asymptotically long times; in the real world, it continues to time scales of 10-30 years
 62 (industrial) and 50-100 years (pre-industrial) after which a new $H > 0$ regime is observed; it is natural to associate this new
 63 regime with the climate (see Fig. 5 of Lovejoy et al., 2013; see also Franzke et al., 2013). Other papers analyzing macroweather
 64 scaling include Koscielny-Bunde et al., (1998); Eichner et al., (2003); Kantelhardt et al., (2006); Rybski et al., (2006); Bunde et
 65 al., (2005); Østvand et al., (2014); Rypdal and Rypdal, (2014).

66 The explanation for the “macroweather” to climate transition (at scale τ_c) appears to be that over the “macroweather” time
 67 scales - where the fluctuations are “cancelling” - other, slow processes which presumably include both external climate forcings
 68 and other slow (internal) land-ice or biogeochemical processes – become stronger and stronger. At some point (τ_c) their
 69 variability dominates. , from ≈ 80 kyrs to ≈ 500 kyrs) and “megaclimate” regimes ($H > 0$, from 500 kyrs to at least 550 Myrs;

70 see A significant point where opinions diverge is the value of the global transition scale τ_c during the preindustrial
 71 Holocene; see (Lovejoy, 2015a) for a discussion.

72 **1.3 Scaling in the numerical models**

73 There have been several studies of the low frequency control run responses of GCMs (Vyushin et al., 2004; Zhu et al., 2006;
 74 Fraedrich et al., 2009; Lovejoy et al., 2013) finding that they are scaling down to their lowest frequencies. This scaling is a
 75 consequence of the absence of a characteristic time scale for the long-time model convergence; it turns out that the relevant
 76 scaling exponents are very small: empirically the GCM convergence is “ultra slow” (Lovejoy et al., 2013) (section 3.4). Most
 77 earlier studies focused on the implications of the long – range statistical dependencies implicit in the scaling statistics.
 78 Unfortunately, due to this rather technical focus, the broader implications of the scaling have not been widely appreciated.

79 More recently, using scaling fluctuation analysis, behavior has been put into the general theoretical framework of GCM
 80 climate modeling (Lovejoy et al., 2013). From the scaling point of view, it appears that the climate arises as a consequence of
 81 slow internal climate processes combined with external forcings (especially volcanic and solar - and in the recent period -
 82 anthropogenic forcings). From the point of view of the GCMs, the low frequency (multicentennial) variability arises exclusively
 83 as a response to external forcings, although potentially - with the addition of (known or currently unknown) slow processes such
 84 as land-ice or biogeochemical processes - new internal sources of low frequency variability could be included. Ignoring the
 85 recent (industrial) period, and confining ourselves to the last millennium, the key question for GCM models is whether or not
 86 they can reproduce the climate regime where the decline of the “macroweather” fluctuations ($H < 0$) is arrested and the
 87 increasing $H > 0$ climate regime fluctuations begin. In a recent publication (Lovejoy et al., 2013), four GCMs simulating the
 88 last millennium were statistically analyzed and it was found that their low frequency variability (especially below $(100 \text{ yrs})^{-1}$)
 89 was somewhat weak, and this was linked to both the weakness of the solar forcings (when using sunspot-based solar
 90 reconstructions with $H > 0$), and – for strong volcanic forcings - with the statistical type of the forcing ($H < 0$, Lovejoy and
 91 Schertzer, 2012a; Bothe et al., 2013a,b; Zanchettin et al., 2013; see also Zanchettin et al., 2010 for the dynamics on centennial
 92 time scales).

93 **1.4 This paper**

94 The weakness of the responses to solar and volcanic forcings at multicentennial scales raises question a linearity question: is the
 95 response of the combined (solar plus volcanic) forcing roughly the sum of the individual responses? Additivity is often implicitly
 96 assumed when climate forcings are reduced to their equivalent radiative forcings and Mann et al., (2005) already pointed out that
 97 – at least - in the Zebiac-Cane (ZC) model discussed below that they are not additive. Here we more precisely analyze this
 98 question and quantify the degree of sub-additivity as a function of temporal scale (section 3.4). A related linear/nonlinear issue
 99 pointed out by Clement et al., (1996), is that due to the nonlinear model response, there is a high sensitivity to a small forcing
 100 and a low sensitivity to a large forcing. Systems in which strong and weak events have different statistical behaviors display
 101 stronger or weaker “clustering” and are often termed “intermittent” (from turbulence). When they are also scaling, the weak and
 102 strong events are characterized by different scaling exponents that quantify how the respective clustering changes with scale. In
 103 section 4, we investigate this quantitatively and confirm that it is particularly strong for volcanic forcing, and that for the ZC
 104 model the response (including that of a GCM), is much less intermittent, implying that the model strongly (and nonlinearly)
 105 smooths the forcing.

106 In this paper, we establish analysis methodologies that can address these issues and apply them to model outputs
107 that cover the the required range of time scales: Last Millenium model outputs. Unfortunately - although we consider the NASA
108 GISS E2-R Last Millenium simulations, there seem to be no full Last Millenium GCM simulations that have the entire suite of
109 volcanic only, solar only and solar plus volcanic forcings and responses, therefore we have use the simplified Zebiak-Cane
110 model outputs published by Mann et al., (2005).

111 Although the Zebiak –Cane model lacks several important mechanisms- notably for our purposes deep ocean dynamics -
112 there are clearly sources of low frequency variability present in the model. For example, Goswami and Shukla, (1991) using 360
113 year control runs found multidecadal and multicentennial nonlinear variability due to the feedbacks between SST anomalies, low
114 level convergence and atmospheric heating. In addition, in justifying his Millenium ZC simulations, (Mann et al., 2005)
115 specifically cited model centennial scale variability as a motivating factor.

116 2. Data and analysis

117 2.1 Discussion

118 During the pre-industrial part of the last millennium, the atmospheric composition was roughly constant, and the earth’s orbital
119 parameters varied by only a small amount. The main forcings used in GCM climate models over this period are thus solar and
120 volcanic (in the GISS-E2-R simulations discussed below, reconstructed land use changes are also simulated but the
121 corresponding forcings are comparatively weak and will not be discussed further). In particular, the importance of volcanic
122 forcings was demonstrated by Minnis et al., (1993) who investigated the volcanic radiative forcing caused by the 1991 eruption
123 of Mount Pinatubo, and found that volcanic aerosols produced a strong cooling effect. Later, Shindell et al., (2003) used a
124 stratosphere-resolving general circulation model to examine the effect of the volcanic aerosols and solar irradiance variability on
125 pre-industrial climate change. They found that the best agreement with historical and proxy data was obtained using both
126 forcings. However, solar and volcanic forcings induce different responses because the stratospheric and surface influences in the
127 solar case reinforce one another but in the volcanic case they are opposed. In addition, there are important differences in solar
128 and volcanic temporal variabilities (including seasonality) that statistically link volcanic eruptions with the onset of ENSO events
129 (Mann et al., 2005). Decreased solar irradiance cools the surface and stratosphere (Kondratyev and Varotsos, 1995). In contrast,
130 volcanic eruptions cool the surface, but aerosol heating warms the sunlit lower stratosphere (Shindell et al., 2003; Miller et al.,
131 2012). This leads to an increased meridional gradient in the lower stratosphere, but a reduced gradient in the tropopause region
132 (Chandra et al., 1996; Varotsos et al., 2004).

133 Vyushin et al., (2004) suggested that volcanic forcings improve the low frequency variability scaling performance of
134 atmosphere-ocean models compared to all other forcings (see however the comment by Blender and Fraedrich, (2004), which
135 also discusses earlier papers on the field e.g. Fraedrich and Blender, (2003); Blender and Fraedrich, (2004). Weber, (2005) used
136 a set of simulations with a climate model, driven by reconstructed forcings in order to study the Northern Hemisphere
137 temperature response to volcanic and solar forcing, during 1000-1850. It was concluded that the response to solar forcing
138 equilibrates at interdecadal timescales, while the response to volcanic forcing never equilibrates due to the fact that the time
139 interval between volcanic eruptions is typically shorter than the dissipation time scale of the climate system (in fact they are
140 scaling so that eruptions occur over all observed time scales, see below).

141 At the same time, Mann et al. (2005) investigated the response of El Niño to natural radiative forcing changes
 142 during 1000-1999, by employing the Zebiak–Cane model for the coupled ocean–atmosphere system in the tropical Pacific. They
 143 found that the composite feedback of the volcanic and solar radiative forcing to past changes, reproduces the fluctuations in the
 144 variability of the historic El Niño records.

145 Finally, as discussed below Lovejoy and Schertzer, (2012a) analysed the time scale dependence of several solar
 146 reconstructions Lean, (2000); Wang et al., (2005); Krivova et al., (2007); Steinhilber et al., (2009); Shapiro et al., (2011) and the
 147 two main volcanic reconstructions Crowley, (2000) and Gao et al., (2008), (referred to as “Crowley” and “Gao” in the following).
 148 The solar forcings were found to be qualitatively quite different depending on whether the reconstructions were based on
 149 sunspots or ^{10}Be isotopes from ice cores with the former increasing with time scale and the latter decreasing with time scale. This
 150 quantitative and qualitative difference brings into question the reliability of the solar reconstructions. By comparison, the two
 151 volcanic reconstructions were both statistically similar in type; they were very strong at annual and sometimes multiannual scales
 152 but they quickly decrease with time scale ($H < 0$) explaining why they are weak at centennial and millennial scales. We re-
 153 examine these findings below.

154 2.2 The climate simulation of Mann et al. (2005) using the Zebiak-Cane model

155 Mann et al., (2005) used the Zebiak–Cane model of the tropical Pacific coupled ocean – atmosphere system (Zebiak and Cane,
 156 1987) to produce a 100-realization ensemble for solar forcing only, volcanic forcing only and combined forcings over the last
 157 millennium. Figure 1a shows the forcings and mean responses of the model which were obtained from:
 158 ftp://ftp.ncdc.noaa.gov/pub/data/paleo/climate_forcing/mann2005/mann2005.txt. No anthropogenic effects were included. Mann
 159 et al. [2005] modeled the region between $\pm 30^\circ$ of latitude - by scaling the Crowley volcanic forcing reconstruction with a
 160 geometric factor 1.57 to take the limited range of latitudes into account. Figure 1b shows the corresponding GISS-E2-R
 161 simulation responses for three different forcings as discussed in Schmidt et al., (2013) and Lovejoy et al., (2013). Although these
 162 were averaged over the northern hemisphere land only (a somewhat different geography than the ZC simulations), one can see
 163 that the low frequencies seem similar even if the high frequencies are somewhat different. We quantify this below.

164 3. Methods

165 3.1 Comparing simulations with observations as functions of scale

166 The ultimate goal of weather and climate modelling (including forecasting) is to make simulations $T_{sim}(t)$ as close as possible to
 167 observations $T_{obs}(t)$. Ignoring measurement errors and simplifying the discussion by only considering a single spatial location
 168 (i.e. a single time series), the goal is to achieve simulations with $T_{sim}(t) = T_{obs}(t)$. However, this is not only very ambitious for the
 169 simulations, even when considering the observations, $T_{obs}(t)$ is often difficult to evaluate if only because data are often sparse or
 170 inadequate in various ways. However, a necessary condition for $T_{sim}(t) = T_{obs}(t)$ is the weaker statistical equality: $T_{sim}(t) \stackrel{d}{=} T_{obs}(t)$ where
 171 “ $\stackrel{d}{=}$ ” means equal in probability distributions (we can say that $a \stackrel{d}{=} b$ if $\Pr(a > s) = \Pr(b > s)$ where “Pr” indicates “probability”).
 172 Although $T_{sim}(t) \stackrel{d}{=} T_{obs}(t)$ is only a necessary (but not sufficient) condition for $T_{sim}(t) = T_{obs}(t)$, it is much easier to empirically verify.

Starting in the 1990s, with the advent of ensemble forecasting systems, the Rank Histogram (RH) method was proposed (Anderson, 1996) as a simple nonparametric test of $T_{sim}(t) \stackrel{d}{=} T_{obs}(t)$, and this has led to a large literature, including recently Bothe et al., (2013a, b). From our perspective there are two limitations of the RH method. First, it is non-parametric so that its statistical power is low. More importantly, it essentially tests the equation $T_{sim}(t) \stackrel{d}{=} T_{obs}(t)$ at a single unique time scale/resolution. This is troublesome since the statistics of both $T_{sim}(t)$ and $T_{obs}(t)$ series will depend on their space-time resolutions; recall that averaging in space alters the temporal statistics, e.g. $5^\circ \times 5^\circ$ data are not only spatially, but also are effectively temporally smoothed with respect to $1^\circ \times 1^\circ$ data. This means that even if $T_{sim}(t)$ and $T_{obs}(t)$ have nominally the same temporal resolutions they may easily have different high frequency variability. Possibly more importantly - as claimed in Lovejoy et al., (2013) and below - the main difference between $T_{sim}(t)$ and $T_{obs}(t)$ may be that the latter has more low frequency variability than the former, and this will not be captured by the RH technique which operates only at the highest frequency available. This problem is indirectly acknowledged, see for example the discussion of correlations in Marzban et al., (2011). The potential significance of the low frequencies becomes obvious when $H > 0$ for the low frequency range. In this case – since the series tends to “wander”, small differences in the low frequencies may translate into very large differences in RH, and this even if the high frequencies are relatively accurate.

A straightforward solution is to use the same basic idea – i.e. to change the sense of equality from deterministic to probabilistic (“=” to “ $\stackrel{d}{=}$ ”) – but to compare the statistics systematically over a range of time scales. The simplest way is to check the equality $\Delta T_{sim}(\Delta t) \stackrel{d}{=} \Delta T_{obs}(\Delta t)$ where ΔT is the fluctuation of the temperature over a time period Δt (see the discussion in Lovejoy and Schertzer, (2013) box 11.1). In general, knowledge of the probabilities is equivalent to knowledge of (all) the statistical moments (including the non-integer ones), and for technical reasons it turns out to be easier to check $\Delta T_{sim}(\Delta t) \stackrel{d}{=} \Delta T_{obs}(\Delta t)$ by considering the statistical moments.

3.2 Scaling Fluctuation Analysis

In order to isolate the variability as a function of time scale Δt , we estimated the fluctuations $\Delta F(\Delta t)$ (forcings, W/m^2), $\Delta T(\Delta t)$ (responses, K). Although it is traditional (and often adequate) to define fluctuations by absolute differences $\Delta T(\Delta t) = |T(t + \Delta t) - T(t)|$, for our purposes this is not sufficient. Instead we should use the absolute difference of the means from t to $t + \Delta t / 2$ and from $t + \Delta t / 2$ to $t + \Delta t$. Technically, the latter corresponds to defining fluctuations using Haar wavelets rather than “poor man’s” wavelets (differences). In a scaling regime, the fluctuations vary with the time lag in a power law manner:

$$\Delta T = \varphi \Delta t^H \quad (1)$$

where φ is a controlling dynamical variable (e.g. a dynamical flux) whose mean $\langle \varphi \rangle$ is independent of the lag Δt (i.e. independent of the time scale). This means that the behaviour of the mean fluctuation is $\langle \Delta T \rangle \approx \Delta t^H$ so that when $H > 0$, on average fluctuations tend to grow with scale whereas when $H < 0$, they tend to decrease. Note that the symbol “ H ” is in honour of Harold Edwin Hurst (Hurst, 1951). Although in the case of quasi-Gaussian statistics, it is equal to his eponymous exponent, the H used here is valid in the more general multifractal case and is generally different.

205 Fluctuations defined as differences are adequate for fluctuations increasing with scale ($H > 0$). When $H > 0$, the rate
 206 at which average differences increase with time lag Δt directly reflects the increasing importance of low frequencies with
 207 respect to high frequencies. However, in physical systems the differences tend to increase even when $H < 0$. This is because
 208 correlations $\langle T(t + \Delta t)T(t) \rangle$ tend to decrease with the time lag Δt and this directly implies that the mean square differences
 209 $\langle \langle \Delta T(\Delta t)^2 \rangle \rangle$ increase (mathematically, for a stationary process: $\langle \Delta T(\Delta t)^2 \rangle = \langle (T(t + \Delta t) - T(t))^2 \rangle = 2(\langle T^2 \rangle - \langle T(t + \Delta t)T(t) \rangle)$.
 210 This means that when $H < 0$, differences cannot correctly characterize the fluctuations. For $H < 0$ the high-frequency details
 211 dominate the differences and prevent these differences to decrease with increasing scale Δt .

212 The Haar fluctuation which is useful for $-1 < H < 1$ is particularly easy to understand since with proper “calibration” in
 213 regions where $H > 0$, its value can be made to be very close to the difference fluctuation, while in regions where $H < 0$, it can
 214 be made close to another simple to interpret “anomaly fluctuation”. The latter is simply the temporal average of the series over a
 215 duration Δt of the series with its overall mean removed (in Lovejoy and Schertzer, 2012b this was termed a “tendency”
 216 fluctuation which is a less intuitive term). In this case, the decrease of the Haar fluctuations for increasing lag Δt characterizes
 217 how effectively averaging a (mean zero) process (the anomaly) over longer time scales reduces its variability. Here, the
 218 calibration is affected by multiplying the raw Haar fluctuation by a factor of 2 which brings the values of the Haar fluctuations
 219 very close to both the corresponding difference and anomaly fluctuations (over time scales with $H > 0$, $H < 0$ respectively).
 220 This means that in regions where $H > 0$, to good accuracy, the Haar fluctuations can be treated as differences whereas in regions
 221 where $H < 0$ they can be treated as anomalies. While other techniques such as Detrended Fluctuation Analysis (Peng et al.,
 222 1994) perform just as well for determining exponents, they have the disadvantage that their fluctuations are not at all easy to
 223 interpret (they are the standard deviations of the residues of polynomial regressions on the running sum of the original series).

224 Once estimated, the variation of the fluctuations with time scale can be quantified by using their statistics; the q^{th} order
 225 structure function $S_q(\Delta t)$ is particularly convenient:

$$226 \quad S_q(\Delta t) = \langle \Delta T(\Delta t)^q \rangle \quad (2)$$

227 where “ $\langle \rangle$ ” indicates ensemble averaging (here, we average over all disjoint intervals of length Δt). Note that although q can in
 228 principle be any value, here we restrict to $q > 0$ since divergences may occur – indeed for multifractals, are expected - for $q < 0$). In
 229 a scaling regime, $S_q(\Delta t)$ is a power law:

$$230 \quad S_q(\Delta t) = \langle \Delta T(\Delta t)^q \rangle \propto \Delta t^{\xi(q)}; \quad \xi(q) = qH - K(q) \quad (3)$$

231 where the exponent $\xi(q)$ has a linear part qH and a generally nonlinear and convex part $K(q)$ with $K(1)=0$. $K(q)$ characterizes
 232 the strong non Gaussian, multifractal variability; the “intermittency”. Gaussian processes have $K(q)=0$. The root-mean-square
 233 (RMS) variation $S_2(\Delta t)^{1/2}$ (denoted simply $S(\Delta t)$ below) has the exponent $\xi(2)/2 = H - K(2)/2$. It is only when the
 234 intermittency is small ($K(q) \approx 0$) that we have $\xi(2)/2 \approx H = \xi(1)$. Note that since the spectrum is a second order statistic, we have the
 235 useful relationship for the exponent β of the power law spectra: $\beta = 1 + \xi(2) = 1 + 2H - K(2)$ (this is a corollary of the Wiener-
 236 Khintchin theorem). Again, only when $K(2)$ is small do we have the commonly used relation $\beta \approx 1 + 2H$; in this case, $H > 0$,
 237 $H < 0$ corresponds to $\beta > 1$, $\beta < 1$ respectively. To get an idea of the implications of the nonlinear $K(q)$, note that a high q value

characterizes the scaling of the strong events whereas a low q characterizes the scaling of the weak events (q is not restricted to integer. The scalings are different whenever the strong and weak events cluster to different degrees, the clustering in turn is precisely determined by another exponent - the codimension - which is itself is uniquely determined by $K(q)$. We return to the phenomenon of “intermittency”, in section 4, it is particularly pronounced in the case of volcanic forcings.

Figure 2a shows the result of estimating the Haar fluctuations for the solar and volcanic forcings. The solar reconstruction that was used is a hybrid obtained by “splicing” the annual resolution sunspot based reconstruction (Fig. 2b, top; back to 1610, although only the more recent part was used by Mann et al. (2005)) with a ^{10}Be based reconstruction (Fig. 2b, bottom) at much lower resolution ($\approx 40\text{-}50$ yrs). In Fig. 2a, the two rightmost curves are for two different ^{10}Be reconstructions; at any given time scale, their amplitudes differ by nearly a factor of 10 yet they both have Haar fluctuations that diminish with scale ($H \approx -0.3$). Figure 2b (top) clearly shows the qualitative difference with “wandering” ($H > 0$, sunspot based) and Fig. 2b (bottom), the cancelling ($H < 0$, ^{10}Be based) solar reconstructions (Lovejoy and Schertzer, 2012a). In the “spliced” reconstruction used here, the early ^{10}Be part (1000-1610) at low resolution was interpolated to annual resolution; the interpolation was close to linear so that we find $H \approx 1$ over the scale range 1-50 yrs, with the $H < 0$ part barely visible over the range 100-600 years (roughly the length of the ^{10}Be part of the reconstruction).

The reference lines in Fig. 2a have slopes -0.4, -0.3, 0.4 showing that both solar and volcanic forcings are fairly accurately scaling (although because of the “splicing” for the solar, only up until $\approx 200\text{-}300$ yrs) but with exactly opposite behaviours: whereas the solar fluctuations increase with time scale, the volcanic fluctuations decrease with scale. For time scales beyond 200-300 yrs, the solar forcing is stronger than the volcanic forcing (they “cross” at roughly 0.3 W/m^2).

3.3 Linearity and nonlinearity

There is no question that - at least in the usual deterministic sense - the atmosphere is turbulent and nonlinear. Indeed, the ratio of the nonlinear to the linear terms in the dynamical equations - the Reynolds number - is typically about 10^{12} . Due to the smaller range of scales, in the numerical models it is much lower, but it is still $\approx 10^3$ to 10^4 . Indeed it turns out that the variability builds up scale by scale from large to small scales so that - since the dissipation scale is about 10^{-3} m - the resulting (millimetre scale) variability can be enormous; the statistics of this buildup are quite accurately modelled by multifractal cascades (see the review Lovejoy and Schertzer, 2013, especially ch. 4 for cascade analyses of data and model outputs). The cascade based Fractionally Integrated Flux model (FIF, Schertzer and Lovejoy, 1987) is a nonlinear stochastic model of the weather scale dynamics, and can be extended to provide nonlinear stochastic models of the macroweather and climate regimes (Lovejoy and Schertzer, 2013, ch. 10).

However, ever since Hasselmann, (1976), it has been proposed that sufficiently space-time averaged variables may respond linearly to sufficiently space-time averaged forcings. In the resulting (low frequency) phenomenological models, the nonlinear deterministic (high frequency) dynamics act as a source of random perturbations; the resulting stochastic model is usually taken as being linear. Such models are only justified if there is a physical scale separation between the high frequency and low frequency processes. The existence of a relevant break (at 2- 10 day scales) has been known since Panofsky and Van der Hoven, (1955) and was variously theorized as the “scale of migratory pressure systems of synoptic weather map scale” (Van der Hoven, 1957) and later as the “synoptic maximum” (Kolesnikov and Monin, 1965). From the point of view of Hasselman-type linear stochastic modelling (now often referred to as “Linear Inverse Modelling (LIM)”, e.g., Penland and Sardeshmukh, (1995); Newman et al., (2003); Sardeshmukh and Sura, (2009)), the system is regarded as a multivariate Ornstein-Uhlenbeck (OU)

275 process. At high frequencies, an OU process is essentially the integral of a white noise (with spectrum $\omega^{-\beta_h}$ with $\beta_h = 2$),
 276 whereas at low frequencies it is a white noise, (i.e. ω^{β_l} with $\beta_l = 0$). In the LIM models, these regimes correspond to the weather
 277 and macroweather, respectively. Recently Newman, (2013) has shown predictive skill for global temperature hindcasts is
 278 somewhat superior to GCM's for 1-2 year horizons.

279 In the more general scaling picture going back to Lovejoy and Schertzer, (1986), the transition corresponds to the lifetime
 280 of planetary structures. This interpretation was quantitatively justified in (Lovejoy and Schertzer, 2010) by using the turbulent
 281 energy rate density. The low and high frequency regimes were scaling and had spectra significantly different than those of OU
 282 processes (notably with $0.2 < \beta_l < 0.8$) with the two regimes now being referred to as “weather” and “macroweather” (Lovejoy and
 283 Schertzer, 2013). Indeed, the main difference with respect to the classical LIM is at low frequencies. Although the difference in
 284 β_l may not seem so important, the LIM value $\beta_l = 0$, (white noise) has no low frequency predictability whereas the actual
 285 values $0.2 < \beta_l < 0.8$ (depending mostly on the land or ocean location) corresponds to potentially huge predictability (the latter can
 286 diverge as β_l approaches 1). A new “ScaLIing Macroweather Model” (SLIMM) has been proposed as a set of fractional order
 287 (but still linear) stochastic differential equations with predictive skill for global mean temperatures out to at least 10 years
 288 (Lovejoy et al., 2015; Lovejoy, 2015b). However, irrespective of the exact statistical nature of the weather and macroweather
 289 regimes, a linear stochastic model may still be a valid approximation over significant ranges.

290 These linear stochastic models (whether LIM or SLIMM) explicitly exploit the weather/macroweather transition and may
 291 have some skill up to macroweather scales perhaps as large as decades. However, at longer time scales, another class of
 292 phenomenological model is often used, wherein the dynamics are determined by radiative energy balances. Energy balance
 293 models focus on slower (true) climate scale processes such as sea ice – albedo feedbacks and are generally quite nonlinear, being
 294 associated with nonlinear features such as tipping points and bifurcations (Budyko, 1969). These models are typically zero or one
 295 dimensional in space (i.e. they are averaged over the whole earth or over latitude bands) and may be deterministic or stochastic
 296 (see (Nicolis, 1988) for an early comparison of the two approaches). See Dijkstra, (2013) for a survey of the classical
 297 deterministic dynamical systems approach as well as the more recent stochastic “random dynamical systems” approach, (see also
 298 Ragone, et al., 2014)

299 Although energy balance models are almost always nonlinear, there have been several suggestions that linear energy
 300 balance models are in fact valid up to millennial and even multimillennial scales. Finally, we could mention the existence of
 301 empirical evidence of stochastic linearity between forcings and responses in the macroweather regime. Such evidence comes for
 302 example, from the apparent ability of linear regressions to “remove” the effects of volcanic, solar and anthropogenic forcings
 303 (Lean and Rind, 2008). This has perhaps been quantitatively demonstrated in the case of anthropogenic forcing where use is
 304 made of the globally, annually averaged CO_2 radiative forcings (as a linear surrogate for all anthropogenic forcings). When this
 305 radiative forcing was regressed against similarly averaged temperatures, it gave residues with amplitudes $\pm 0.109\text{K}$ (Lovejoy,
 306 2014a) which is almost exactly the same as GCM estimates of the natural variability (e.g., Laepple et al., (2008)). Notice that in
 307 this case the identification of the global temperature T_{globe} as the sum of a regression determined anthropogenic component (T_{anth})
 308 with residues as natural variability (T_{nat}) is in fact only a confirmation of *stochastic* linearity (i.e. $T_{\text{globe}} \stackrel{d}{=} T_{\text{anth}} + T_{\text{nat}}$). Since
 309 presumably the actual residues would have been different if there had been no anthropogenic forcing. Indeed, when the residues
 310 were analysed using fluctuation analysis, it was only their statistics that were close to the pre-industrial multiproxy statistics.

3.4 Testing linearity: the additivity of the responses

We can now test the linearity of the model responses to solar and volcanic forcings. First consider the model responses (Fig. 3a). Compare the response to the volcanic only forcing (green) curve; with the response from the solar only forcing (black). As expected from Fig. 2a, the former is stronger than the latter up (until centennial scales) reflecting the stronger volcanic forcing. At scales $\Delta t \approx 100$ yrs however, we see that the solar only has a stronger response, also as expected from Fig. 2a. Now consider the response to the combined volcanic and solar forcing (brown). Unsurprisingly, it is very close to the volcanic only until $\Delta t \approx 100$ yrs; however at longer time scales, the combined response seems to decrease following the volcanic forcing curve; it seems that at these longer time scales the volcanic and solar forcings have negative feedbacks so that the combined response to solar plus volcanic forcing is actually less than for pure solar forcing, they are “subadditive”.

In order to quantify this we can easily determine the expected solar and volcanic response if the two were combined additively (linearly). In the latter case, the solar and volcanic fluctuations would not interfere with each other, and since forcings are statistically independent, the responses would also be statistically independent, the response variances would add.

A linear response means that temperature fluctuations due to only solar forcing ($\Delta T_s(\Delta t)$) and only volcanic forcing ($\Delta T_v(\Delta t)$) would be related to the temperature fluctuations of the response to the combined solar plus volcanic forcings ($\Delta T_{s,v}(\Delta t)$) as:

$$\Delta T_{s,v}(\Delta t) = \Delta T_s(\Delta t) + \Delta T_v(\Delta t) \quad (4)$$

This is true regardless of the exact definition of the fluctuation: as long as the fluctuation is defined by a linear operation on the temperature series any wavelet will do. Therefore, squaring both sides and averaging (“ $\langle \rangle$ ”) and assuming that the fluctuations in the solar and volcanic forcings are statistically independent of each other (i.e., $\langle \Delta T_s(\Delta t) \Delta T_v(\Delta t) \rangle = 0$), we obtain:

$$\langle \Delta T_{s,v}(\Delta t)^2 \rangle = \langle \Delta T_s(\Delta t)^2 \rangle + \langle \Delta T_v(\Delta t)^2 \rangle \quad (5)$$

The implied additive response structure function $S_{(\Delta t)} = \left(\langle \Delta T_s(\Delta t)^2 \rangle + \langle \Delta T_v(\Delta t)^2 \rangle \right)^{1/2}$ is shown in Fig. 3b along with the ratio of the latter to the actual (nonlinear) solar plus volcanic response (top: $\left(\langle \Delta T_s(\Delta t)^2 \rangle + \langle \Delta T_v(\Delta t)^2 \rangle \right)^{1/2} / \langle \Delta T_{s,v}(\Delta t)^2 \rangle^{1/2}$). It can be seen that the ratio is fairly close to unity for time scales below about 50 yrs. However beyond 50 yrs there is indeed a strong negative feedback between the solar and volcanic forcings. This is seen more clearly in Fig. 3c which shows that at $\Delta t \approx 400$ years, that the negative feedback is strong enough to reduce the theoretical additive fluctuation amplitudes by a factor of ≈ 2.5 (the fall-off at the largest Δt is probably an artefact of the poor statistics at these scales). It should be noted that the latter holds assuming independence (pink curve in Fig. 3c) of the solar and volcanic forcing. For comparison, the purple curve in Fig. 3c illustrates the results obtained when analyzing the series constructed by directly summing the two response series (instead of assuming statistical independence). It is clearly seen that the basic result still holds but it is a little less strong (a factor of ≈ 2). The reason for the difference is that the cancellation of the cross terms assumed by statistical independence is only approximately valid on simple realizations, especially at the lower frequencies where the statistics are worse.

In the ZC model, all forcings are input at the surface so that here the subadditivity is due to the differing seasonality, fluctuation intensities and spatial distributions of the solar and volcanic forcings. In the GISS-E2-R GCM simulations, the response to the solar forcing is too small to allow us to determine if it involves a similar solar-volcanic negative feedback (Fig. 4). In GCMs with their vertically stratified atmospheres or the real atmosphere, non additivity is perhaps not surprising given the

346 difference between the solar and volcanic vertical heating profiles. If such negative feedbacks are substantiated in
 347 further simulations, it would enhance the credibility of the idea that current GCMs are missing critical slow (multi centennial,
 348 multi millennial) climate processes. No matter what the exact explanation, non additivity underlines the limitations of the
 349 convenient reduction of climate forcings to radiative forcing equivalents. It also indicates that at scales longer than about 50 yrs
 350 energy budget models must nonlinearly account for albedo-temperature interactions (i.e. that linear energy budget models are
 351 inadequate at these time scales, and that albedo-temperature interactions must at least be correctly parametrized).

352 Also shown for reference in Fig. 3a are the fluctuations for three multiproxy estimates of annual northern hemisphere
 353 temperatures (1500-1900; pre-industrial, Moberg et al., 2005; Huang, 2004; Ljungqvist, 2010, the analysis was taken from
 354 Lovejoy and Schertzer, 2012c). Although it should be borne in mind that the ZC model region (the Pacific) does not coincide
 355 with the proxy region (the northern hemisphere), the latter is the best model validation available. In addition, since we compare
 356 model and proxy fluctuation statistics as functions of time scale, the fact that the spatial regions are somewhat different is less
 357 important than if we had attempted a direct year by year comparison of model outputs with the multiproxy reconstructions.

358 In Fig. 3a, we see that the responses of the volcanic only and the combined volcanic and solar forcings fairly well
 359 reproduce the RMS multiproxy statistics until ≈ 50 yrs; however at longer time scales, the model fluctuations are substantially
 360 too weak – roughly 0.1 K (corresponding to ± 0.05 K) and constant or falling, whereas at 400 yr scales, the RMS multiproxy
 361 temperature fluctuations are ≈ 0.25 K (± 0.125) and rising. Indeed, in order to account for the ice ages, they must continue to rise
 362 until ≈ 5 K (± 2.5 K) at glacial-interglacial scales of 50 – 100 kyrs, (according to paleodata, this rise continues in a smooth, power
 363 law manner with $H > 0$ until roughly 100 kyrs, see Lovejoy and Schertzer, 1986, Shackleton and Imbrie, 1990 Pelletier, 1998,
 364 Schmitt et al., 1995, Ashkenazy et al., 2003, Huybers and Curry, 2006, and Lovejoy et al., 2013).

365 In Fig. 4, we compare the RMS Haar fluctuations from the ZC model combined (volcanic and solar forcing) response
 366 with those from simulations from the GISS-E2-R GCM with solar only forcing and a control run (no forcings, black; see
 367 Lovejoy et al., (2013) for details; the GISS-E2-R solar forcing was the same as the spliced series used in the ZC simulations).
 368 We see that the three are remarkably close over the entire range; for the GISS model, this indicates that the solar only forcing is
 369 so small that the response is nearly the same as for the unforced (control) run. The ZC combined solar and volcanic forcing is
 370 clearly much weaker than the pre-industrial multiproxies (dashed blue, same as in Fig. 3a). The reference line with slope -0.2
 371 shows the convergence of the control to the model climate; the shallowness of the slope (-0.2) implies that the convergence is
 372 ultra slow. For example, fluctuations from a 10 yr run control run are only reduced by a factor of $(10/3000)^{-0.2} \approx 3$ if the run is
 373 extended to 3 kyrs.

374 Finally, in Fig. 5, we compare the responses to the volcanic forcings for the Zebiak-Cane model and for the GISS-E2-R
 375 GCM for two different volcanic reconstructions (Gao et al., 2008), and Crowley, 2000) (the reconstruction used in the ZC
 376 simulation). For reference, we again show the combined ZC response and the preindustrial multiproxies. We see that the GISS
 377 GCM is much more sensitive to the volcanic forcing than the Zebiak-Cane model; indeed, it is too sensitive at scales $\Delta t \approx 100$, but
 378 nevertheless becomes too weak at scales $\Delta t \approx 200$ years. Indeed, since the volcanic forcings continue to decrease with scale, we
 379 expect the responses to keep diminishing with scale at larger Δt .

380 Note that the spatial regions covered by the ZC simulation, the GISS outputs and the multiproxy reconstructions are not
 381 the same. For the latter, the reason is that there is no perfectly appropriate (regionally defined) multiproxy series whereas for the
 382 GISS outputs, we reproduced the structure function analysis from a published source. Yet, the differences in the regions may not
 383 be so important since we are only making statistical comparisons. This is especially true since all the series are for planetary

384 scale temperatures (even if they are not identical global sized regions) and in addition, we are mostly interested in the
 385 fifty year (and longer) statistics which may be quite similar.

386 4. Intermittency: a multifractal trace moment analysis

387 4.1 The Trace moment analysis technique

388 In the previous sections we considered the implications of linearity when climate models were forced separately with two
 389 different forcings compared with the response to the combined forcing; we showed that the ZC model was subadditive. However,
 390 linearity also constrains the relation between the fluctuations in the forcings and the responses. For example at least since the
 391 work of Clement et al., (1996), in the context of volcanic eruptions, it has been recognized that the models are typically sensitive
 392 to weak forcing events but insensitive to strong ones, i.e. they are nonlinear, and Mann et al., (2005) noticed this in their ZC
 393 simulations.

394 In a scaling regime, both forcings and responses will be characterized by a hierarchy of exponents (i.e. the function $\xi(q)$
 395 in Eq. 3 or equivalently by the exponent H and the function $K(q)$), the differences in the statistics of weak and strong events are
 396 reflected in these different exponents; high order moments (large q) are dominated by large fluctuations and conversely for low
 397 order moments. The degree of convexity of $K(q)$ quantifies the degree of these nonlinear effects (indeed, how they vary over
 398 time scales Δt). Such “intermittent” behaviour was first studied in the context of turbulence (Kolmogorov, 1962; Mandelbrot,
 399 1974).

400 In order to quantify this, recall that if the system is linear, the response is a convolution of the system Green’s function
 401 with the forcing, in spectral terms it acts as a filter. If it is also scaling, then the filter is a power law: ω^{-H} where ω is the
 402 frequency, (mathematically, if $\widetilde{T(\omega)}$ and $\widetilde{F(\omega)}$ are the Fourier transforms of the response and forcing, for a scaling linear system,
 403 we have: $\widetilde{T(\omega)} \propto \omega^{-H} \widetilde{F(\omega)}$ such a filter corresponds to a fractional integration of order H). In terms of fluctuations this implies:
 404 $\Delta T(\Delta t) = \Delta t^H \Delta F(\Delta t)$ (assuming that the fluctuations are appropriately defined). Therefore, by taking q^{th} powers of both sides and
 405 ensemble averaging, we see that in linear scaling systems we have: $\xi_T(q) = qH + \xi_F(q)$ (c.f. eq. (3) with $\xi_T(q)$ and $\xi_F(q)$ the
 406 structure function exponents for the response and the forcing respectively). If $\xi_T(q)$ and $\xi_F(q)$ only differ by a term linear in q ,
 407 then $K_T(q) = K_F(q)$, so that if over some regime, we find empirically $K_T(q) \neq K_F(q)$ (i.e. the intermittencies are different), then we
 408 may conclude that that the system is nonlinear (note that this result is independent of whether the linearity is deterministic or
 409 only statistical in nature).

410 Let us investigate the nonlinearity of the exponents by returning to Eq. (1), (2) and (3) in more detail. Up until now we
 411 have studied the statistical properties of the forcings and responses using the RMS fluctuations e.g. we have used the following
 412 equation but only for the value $q=2$:

$$413 \quad \langle \Delta T(\Delta t)^q \rangle \propto \langle \varphi_x^q \rangle \Delta t^{qH} = \Delta t^{\xi(q)}; \quad \xi(q) = qH - K(q) \quad (6)$$

414 (see Eq. (1)) the exponent $K(q)$ (implicitly defined in (3)) is given explicitly by:

415
$$\langle \varphi_{\lambda}^q \rangle = \Delta t^{K(q)} \frac{\tau_{\text{eff}}}{\Delta t} \quad (7)$$

416 where τ_{eff} is the effective outer scale of the multifractal cascade process, φ gives rise to the strong variability and λ' is the
417 cascade ratio from this outer scale to the scale of interest Δt .

418 If the driving flux φ was quasi-Gaussian, then $K(q) = 0$, $\xi(q) = qH$ and the exponent $\xi(2) = 2H = \beta - 1$ would be sufficient
419 for a complete characterization of the statistics. However geophysical series are often far from Gaussian, even without statistical
420 analysis, a visual inspection (the sharp spike” of varying amplitudes, see Fig. 1a) of the volcanic series makes it obvious that it is
421 particularly extreme in this regard. We expect - at least in this case - that the $K(q)$ term will readily be quite large (although note
422 the constraint $K(1) = 0$ and the mean of φ (the $q=1$ statistic) is independent of scale). To characterize this, note that since $K(1) = 0$,
423 we have $\xi(1) = H$ and then use the first two derivatives of $\xi(q)$ at $q=1$ to estimate the tangent (linear approximation) to $K(q)$ near
424 the mean (C_1) and the curvature of $K(q)$ near the mean characterized by α . This gives

425
$$\left. \begin{aligned} C_1 &= K'(1) = H - \xi'(1) \\ \alpha &= K''(1) / K'(1) = \xi''(1) / (\xi'(1) - H) \end{aligned} \right\} \quad (8)$$

426 The parameters C_1 , α are particularly convenient since – thanks to a kind of multiplicative central limit theorem - there
427 exist multifractal universality classes (Schertzer and Lovejoy, 1987). For such universal multifractal processes, the exponent
428 function $K(q)$ can be entirely (i.e. not only near $q=1$) characterized by the same two parameters:

429
$$K(q) = \frac{C_1}{\alpha - 1} (q^\alpha - q); \quad 0 \leq \alpha \leq 2 \quad (9)$$

430 In the universality case (9), it can be checked that the estimate in (8) (near the mean) is satisfied so that C_1 , α
431 characterize all the statistical moments (actually, (6), (7) are only valid for $q < q_c$; for $q > q_c$, the above will break down due to
432 multifractal phase transitions; the critical q_c is typically > 2 , so that here we confine our analyses to $q \leq 2$ and do not discuss the
433 corresponding extreme - large q - behaviour).

434 A drawback with using the above fluctuation method for using $\xi(q)$ to estimate $K(q)$ (6) is that if C_1 is not too big, then
435 for the low order moments q , the exponent $\xi(q)$ may be dominated by the linear (qH) term, so that the multifractal part
436 ($K(q)$) of the scaling is not too apparent. A simple way of directly studying $K(q)$ is to transform the original series so as to
437 estimate the flux φ at a small scale, essentially removing the (qH) part of the exponent. It can then be degraded by temporal
438 averaging and the scaling of the various statistical moments - the exponents $K(q)$ - can be estimated directly. To do this, we
439 divide (1) by its ensemble average so as to estimate the normalized flux at the highest resolution by:

440
$$\varphi' = \frac{\varphi}{\langle \varphi \rangle} = \frac{\Delta T}{\langle \Delta T \rangle} \quad (10)$$

441 where the ensemble average (“ $\langle \rangle$ ”) is estimated by averaging over the available data (here a single series), and the fluctuations
442 Δt are estimated at the finest resolution (here 1 yr).

443

4.2 Trace moment analysis of forcings, responses and multiproxies

We now test (7); for convenience, we use the symbol λ as the ratio of a convenient reference scale – here the length of the series, $\tau_{ref}=1000$ yrs to the resolution scale Δt (for some analyses, 400 yrs was used instead, see the captions in Fig. 6). In an empirical study, the outer scale τ_{eff} is not known a priori, it must be empirically estimated; denote the scale at which the cascade starts by λ'

Starting with (7), the basic prediction of multiplicative cascades is that the normalized moments ϕ' (10) obey the generic multiscaling relation:

$$M(q) = \langle \phi'^q \rangle = \lambda'^{K(q)} = \left(\frac{\tau_{eff}}{\Delta t} \right)^{K(q)} = \left(\frac{\lambda}{\lambda_{eff}} \right)^{K(q)} ; \lambda' = \frac{\tau_{eff}}{\Delta t} = \frac{\lambda}{\lambda_{eff}} ; \lambda_{eff} = \frac{\tau_{ref}}{\tau_{eff}} \quad (11)$$

We can see that τ_{eff} can readily be empirically estimated since a plot of $\text{Log}_{10}M$ versus $\text{Log}_{10}\lambda$ will have lines (one for each q , slope $K(q)$) converging at the outer scale $\lambda = \lambda_{eff}$ (although for a single realisation such as here, the outer scale will be poorly estimated since clearly for a single sample (series) there is no variability at the longest time scales, there is a single long-term value that generally poorly represents the ensemble mean). Figure 6a shows the results when Δt is estimated by the absolute second difference at the finest resolution. The solar forcing (upper right) was only shown for the recent period (1600-2000) over which the higher resolution sunspot based reconstruction was used, the earlier 1000-1600 part was based on a (too) low resolution ^{10}Be “splice” as discussed above, see Fig. 2b. In the solar plot (upper left), but especially in the volcanic forcing plot (upper right), we see that the scaling is excellent over nearly the entire range (the points are nearly linear) and in addition, the lines plausibly “point” (i.e. cross) at a unique outer scale $\lambda = \lambda_{eff}$ which is not far from the length of the series, see Table 1 for estimates of the corresponding time scales. From these plots we see that the responses to the volcanic forcing “spikiness” (intermittency) are much stronger than to the corresponding responses to the weaker solar “spikiness”. The model atmosphere therefore considerably dampens the intermittency, but also this effect is highly nonlinear so that the intermittency of the combined volcanic and solar forcing (bottom left) is actually a little less than the volcanic only intermittency (bottom right). Table 1 gives a quantitative characterization of the intermittency strength near the mean, using the C_1 parameter.

It is interesting at this stage to compare the intermittency of the ZC outputs with those of the GISS-E2-R GCM (Fig. 6b) and with multiproxy temperature reconstructions (Fig. 6c). In Fig. 6b, we see that the GISS-E2-R trace moments rapidly die off at large scales (small λ) so that the intermittency is limited to small scales to the right of the convergence point. In this Figure, we see that the lines converge at $\text{Log}_{10}\lambda \approx 1.1 - 1.5$ corresponding to τ_{eff} in the range roughly 10–30 yrs. Since the intermittency builds up scale by scale from large scales modulating smaller scales in a hierarchical manner, and since this range of scales is small, the intermittency will be small. The partial exception is for the upper right plot which is for the GISS-E2-R response to the large Gao volcanic forcing (recall that the ZC model uses the weaker, Crowley volcanic reconstruction whose response is strongly intermittent, see Fig. 6b, the upper left plot). This result shows that contrary to the ZC model whose response is strongly intermittent (highly non Gaussian) over most of the range of time scales, the GISS-E2-R response is nearly Gaussian implying that the (highly non Gaussian) forcings are quite heavily (nonlinearly) damped.

This difference in the model responses to the forcing intermittency is already interesting, but it does not settle the question as to which model is more realistic. To attempt to answer this question, we turn to Fig. 6c which shows the trace moment analysis for six multiproxy temperature reconstructions over the same (pre-industrial) period as the GISS-E2-R model (1500-

1900; unlike the ZC model, the GISS-E2-R included anthropogenic forcings so that the period since 1900 was not used in the GISS-E2-R analysis). Statistical comparisons of nine multiproxies were made in ch. 11 of Lovejoy and Schertzer, (2013), (for reasons of space, only six of these are shown in Fig. 6c) where it was found that the pre 2003 multiproxies had significantly smaller multicentennial and lower frequency variability than the more recent multiproxies used as reference in Fig. 4 and 5. However, Fig. 6c shows that the intermittencies are all quite low (with the partial exception of the Mann series, see the upper right plot). This conclusion is supported by the comparison with the red curves. These indicate the generic envelope of trace moments of quasi-Gaussian processes for $q \leq 2$ it shows how the latter converge (at large scales, small λ , to the left) to the flat ($K(q) = 0$) Gaussian limit. We see that the actual lines are only slightly outside this envelope showing that they are only marginally more variable than quasi-Gaussian processes.

The comparison of the GISS-E2-R outputs (Fig. 6b) with the multiproxies (Fig. 6c) indicates that they are both of low intermittency and are more similar to each other than to the ZC multiproxy statistics. One is therefore tempted to conclude that the GISS-E2-R model is more realistic than the ZC model with its much stronger intermittency. However this conclusion may be premature since the low multiproxy and GISS intermittencies may be due to limitations of both the multiproxies and the GISS-E2-R model. Multicentennial and multimillennial scale ice core analyses displays significant paleotemperature intermittency ($C_1 \approx 0.05 - 0.1$, Schmitt et al., 1995 see the discussion in ch. 11 of Lovejoy and Schertzer, 2013) so that the multiproxies may be insufficiently intermittent.

5. Conclusions

From the point of view of GCM's, climate change is a consequence of changing boundary conditions (including composition), the latter are the climate forcings. Since forcings of interest (such as anthropogenic forcings) are often less than 1% of the mean solar input the responses are plausibly linear. This justifies the reduction of the forcings to a convenient common denominator: the "equivalent radiative forcing", a concept which is useful only if different forcings add linearly, if they are "additive". An additional consequence of linearity is that the climate sensitivities are independent of whether the fluctuations in the forcings are weak or strong. Both consequences of linearity clearly have their limits. For example, at millennial and longer scales, energy balance models commonly discard linearity altogether and assume that nonlinear albedo responses to orbital changes are dominant. Similarly, at monthly and annual scales, the linearity of the climate sensitivity has been questioned in the context of sharp, strong volcanic forcings.

In view of the widespread use of the linearity assumption, it is important to quantitatively establish its limits and this can best be done using numerical climate models. A particularly convenient context is provided by the Last Millennium simulations, which (in the preindustrial epoch) are primarily driven by the physically distinct solar and volcanic forcings (forcings due to land use changes are very weak). The ideal would be to have a suite of the responses of fully coupled GCM's which include solar only, volcanic only and combined solar and volcanic forcings so that the responses could be evaluated both individually and when combined. Unfortunately, the optimal set of GCM products are the GISS E2-R millennium simulations with solar only and solar plus volcanic forcing (this suite is missing the volcanic only responses). We therefore also considered the outputs of a simplified climate model, the Zebiac-Cane (ZC) model (Mann et al., 2005) for which the full suite was available.

Following a previous study, we first quantified the variability of the forcings as a function of time scale by considering fluctuations. These were estimated by using the difference between the averages of the first and second halves of intervals Δt

515 (“Haar” fluctuations). This definition was necessary in order to capture the two qualitatively different regimes, namely
 516 those in which the average fluctuations increase with time scale ($H > 0$) and those in which they decrease with scale ($H < 0$).
 517 Whereas the solar forcing was small at annual scales, it generally increased with scale. In comparison, the volcanic forcing was
 518 very strong at annual scales but rapidly decreased, the two becoming roughly equal at about 200 yrs. By considering the response
 519 to the combined forcing we were then able to examine and quantify their non-additivity (nonlinearity). By direct analysis (Fig.
 520 3b, c), it was found that in the ZC model, additivity of the radiative forcings only works up until roughly 50 yr scales; at 400 yr
 521 scales, there are negative feedback interactions between the solar and volcanic forcings that reduce the combined effect by a
 522 factor of $\approx 2 - 2.5$. This “subadditivity” makes their combined effects particularly weak at these scales. Although this result
 523 seems statistically robust for the ZC Millenium simulations, until the source of the nonlinearity is pin-pointed and the results
 524 reproduced with full-blown coupled GCM’s, they must be considered tentative.

525 In order to investigate possible nonlinear responses to sharp, strong events (such as volcanic eruptions), we used the fact
 526 that if the system is linear and scaling, then the difference between the structure function exponents ($\xi(q)$) for the forcings and
 527 responses is itself a linear function of the order of moment q (moments with large q are mostly sensitive to the rare large
 528 values, small q moments are dominated by the frequent low values). By using the trace moment analysis technique, we isolated
 529 the nonlinear part of $\xi(q)$ (i.e. the function $K(q)$) which quantifies the intermittent (multifractal, highly non-Gaussian) part of
 530 the variability (associated with the “spikiness” of the signal). Unsurprisingly we showed that the volcanic intermittency was
 531 much stronger than the solar intermittency, but that in both cases, the model responses were highly smoothed, they were
 532 practically nonintermittent (close to Gaussian) hence that the model responses to sharp, strong events were not characterized by
 533 the same sensitivity as to the more common weaker forcing events.

534 By examining model outputs, we have found evidence that the response of the climate system is reasonably linear with
 535 respect to the forcing up to time scales of 50 yrs at least for weak (i.e. not sharp, intermittent) events. But the sharp, intermittent
 536 events such as volcanic eruptions that occasionally disrupt the linearity at shorter time scales, become rapidly weaker at longer
 537 and longer time scales (with scaling exponent $H \approx -0.3$). In practice, linear stochastic models may therefore be valid from over
 538 most of the macroweather range, from ≈ 10 days to over 50 years. However, given their potential importance, it would be worth
 539 designing specific coupled climate model experiments in order to investigate this further.

540 6. Acknowledgements:

541 The ZC simulation outputs and corresponding solar and volcanic forcings were taken from
 542 ftp://ftp.ncdc.noaa.gov/pub/data/paleo/climate_forcing/mann2005/mann2005.txt. We thank J. Lean (solar data Fig. 2b (top),
 543 Judith.Lean@nrl.navy.mil), A. Shapiro (solar data, Fig. 2b (bottom) Alexander Shapiro, alexander.shapiro@pmodwrc.ch) and G.
 544 Schmidt (the GISS-E2-R simulation outputs, gavin.a.schmidt@nasa.gov) for graciously providing data and model outputs. The
 545 ECHAM5 based Millenium simulations analyzed in table 1 were available from: [https://www.dkrz.de/Klimaforschung-](https://www.dkrz.de/Klimaforschung-en/konsortial-en/millennium-experiments-1?set_language=en)
 546 [en/konsortial-en/millennium-experiments-1?set_language=en](https://www.dkrz.de/Klimaforschung-en/konsortial-en/millennium-experiments-1?set_language=en). Mathematica and MatLab codes for performing the Haar
 547 fluctuation analyses are available from: <http://www.physics.mcgill.ca/~gang/software/index.html>. This work was unfunded, there
 548 were no conflicts of interest.

549 **References**

- 550 Anderson, J. L.: A method for producing and evaluating probabilistic forecasts from ensemble model integrations, *J. Climate*, 9,
551 1518–1530, 1996.
- 552 Ashkenazy, Y., D. Baker, H. Gildor, and Havlin, S.: Nonlinearity and multifractality of climate change in the past 420,000 years,
553 *Geophys. Res. Lett.*, 30, 2146 doi: 10.1029/2003GL018099, 2003
- 554 Blender, R., and Fraedrich, K.: Comment on “Volcanic forcing improves atmosphere–ocean coupled general circulation model
555 scaling performance” by D. Vyushin, I. Zhidkov, S. Havlin, A. Bunde, and S. Brenner, *Geophys. Res. Lett.*, 31, L22213,
556 doi: 10.1029/2004GL020797, 2004.
- 557 Bothe, O., Jungclaus, J. H., and Zanchettin, D.: Consistency of the multi-model CMIP5/PMIP3-past1000 ensemble, *Climate of
558 the Past*, 9 (6), 2471-2487, 2013a.
- 559 Bothe, O., Jungclaus, J. H., Zanchettin, D., and Zorita, E.: Climate of the last millennium: Ensemble consistency of simulations
560 and reconstructions, *Climate of the Past*, 9 (3), 1089-1110, 2013b.
- 561 Bryson, R. A.: The Paradigm of Climatology: An Essay, *Bull. Amer. Meteor. Soc.*, 78, 450-456, 1997.
- 562 Budyko, M. I.: The effect of solar radiation variations on the climate of the earth, *Tellus*, 21, 611-619, 1969.
- 563 Bunde, A., Eichner, J. F., Kantelhardt, J. W., and Havlin, S.: Long-term memory: a natural mechanism for the clustering of
564 extreme events and anomalous residual times in climate records, *Phys. Rev. Lett.*, 94, 1-4 doi:
565 10.1103/PhysRevLett.94.048701, 2005.
- 566 Chandra, S., Varotsos, C., and Flynn, L. E. The mid-latitude total ozone trends in the northern hemisphere, *Geophys Res Lett.*,
567 23(5), 555-558, 1996.
- 568 Clement, A. C., Seager, R., Cane, M. A., and Zebiak, S. E.: An ocean dynamical thermostat, 2190–2196, 1996.
- 569 Crowley, T. J. :Causes of Climate Change Over the Past 1000 Years, *Science*, 289, 270 doi: 10.1126/science.289.5477.270, 2000.
- 570 Dijkstra, H.: *Nonlinear Climate Dynamics*, 357 pp., Cambridge University Press, Cambridge, 2013.
- 571 Eichner, J. F., Koscielny-Bunde, E., Bunde, A., Havlin, S., and Schellnhuber, H.-J.: Power-law persistence and trends in the
572 atmosphere: A detailed study of long temperature records, *Phys. Rev. E*, 68, 046133-046131-046135 doi:
573 10.1103/PhysRevE.68.046133, 2003.
- 574 Fraedrich, K., Blender, R., and Zhu, X.: Continuum Climate Variability: Long-Term Memory, Scaling, and 1/f-Noise,
575 *International Journal of Modern Physics B*, 23, 5403-5416, 2009.,
- 576 Franzke, J., Frank, D., Raible, C. C., Esper, J., and Brönnimann, S.: Spectral biases in tree-ring climate proxies *Nature Clim.
577 Change*, 3, 360-364 doi: 10.1038/Nclimate1816, 2013.,
- 578 Gao, C. G., Robock, A., and Ammann, C.: Volcanic forcing of climate over the past 1500 years: and improved ice core-based
579 index for climate models, *J. Geophys. Res.*, 113, D23111 doi: 10.1029/2008JD010239, 2008.
- 580 Goswami, B. N., and Shukla, J.: Aperiodic Variability in the Cane—Zebiak Model, *J. of Climate*, 6, 628-638, 1991.
- 581 Hansen, J., Sato, M. K. I., Ruedy, R., Nazarenko, L., Lacis, A., Schmidt, G. A., and Bell, N.: Efficacy of climate forcings, *J.
582 Geophys. Res.*, 110, D18104 doi:10.1029/2005JD005776, 2005.
- 583 Hasselmann, K.: Stochastic Climate models, part I: Theory, *Tellus*, 28, 473-485, 1976
- 584 Huang, S.: Merging Information from Different Resources for New Insights into Climate Change in the Past and Future,
585 *Geophys. Res. Lett.*, 31, L13205 doi:10.1029/2004 GL019781, 2004.
- 586 Hurst, H. E.: Long-term storage capacity of reservoirs, *Trans. Amer. Soc. Civil Eng.*, 116, 770-808, 1951.

- 587 Huybers, P., and Curry, W.: Links between annual, Milankovitch and continuum temperature variability, *Nature*, 441,
588 329-332 doi:10.1038/nature04745, 2006.
- 589 Kantelhardt, J. W., Koscielny-Bunde, E., Rybski, D., Braun, P., Bunde, A., and Havlin, S.: Long-term persistence and
590 multifractality of precipitation and river runoff record, *J. Geophys. Res.*, 111 doi: doi:10.1029/2005JD005881, 2006.
- 591 Kolesnikov, V. N., and Monin, A. S.: Spectra of meteorological field fluctuations, *Izvestiya, Atmospheric and Oceanic Physics*,
592 1, 653-669, 1965.,
- 593 Kolmogorov, A. N.: A refinement of previous hypotheses concerning the local structure of turbulence in viscous incompressible
594 fluid at high Reynolds number, *Journal of Fluid Mechanics*, 83, 349, 1962,
- 595 Kondratyev, K. Y., and Varotsos, C. A.: Volcanic eruptions and global ozone dynamics, *Int. J. Remote Sens.*, 16 (10), 1887-
596 1895, 1995.
- 597 Koscielny-Bunde, E., Bunde, A., Havlin, S., Roman, H. E., Goldreich, Y., and Schellnhuber, H. J.: Indication of a universal
598 persistence law governing atmospheric variability, *Phys. Rev. Lett.* , 81, 729-732, 1998.
- 599 Krivova, N. A., Balmaceda, L., and Solanski, S. K.: Reconstruction of solar total irradiance since 1700 from the surface
600 magnetic field flux, *Astron. and Astrophys*, 467, 335-346 doi: 10.1051/0004-6361:20066725, 2007.
- 601 Laepple, T., Jewson, S., and Coughlin, K.: Interannual temperature predictions using the CMIP3 multi-model ensemble mean,
602 *Geophys. Res. Lett.*, 35, L10701, doi:10.1029/2008GL033576, 2008.
- 603 Lean, J. L.: Evolution of the Sun's Spectral Irradiance Since the Maunder Minimum, *Geophys. Research Lett.*, 27, 2425-2428,
604 2000.
- 605 Lean, J. L., and Rind, D. H.: How natural and anthropogenic influences alter global and regional surface temperatures: 1889 to
606 2006, *Geophys. Res. Lett.*, 35, L18701 doi: 10.1029/2008GL034864, 2008.
- 607 Ljungqvist, F. C.: A new reconstruction of temperature variability in the extra - tropical Northern Hemisphere during the last two
608 millennia, *Geografiska Annaler: Physical Geography*, 92 A(3), 339 - 351 doi:10.1111/j .1468 - 0459.2010 .00399.x, 2010.
- 609 Lovejoy, S.: What is climate?, *EOS*, 94, (1), 1 January, p1-2, 2013.
- 610 Lovejoy, S.: Scaling fluctuation analysis and statistical hypothesis testing of anthropogenic warming, *Climate Dyn.*, 42, 2339-
611 2351 doi:10.1007/s00382-014-2128-2, 2014a.
- 612 Lovejoy, S.: A voyage through scales, a missing quadrillion and why the climate is not what ou expect, *Climate Dyn.*, 44, 3187-
613 3210, doi: 10.1007/s00382-014-2324-0, 2014b.,
- 614 Lovejoy, S.: The macroweather to climate transition in the Holocene: regional and epoch to epoch variability (comments on
615 “Are there multiple scaling regimes in Holocene temperature records?”by T. Nilsen, K. Rypdal, and H.-B. Fredriksen),
616 *Earth Syst. Dynam. Discus.*, 6, C1–C10, 2015a.
- 617 Lovejoy, S.: Using scaling for macroweather forecasting including the pause, *Geophys. Res. Lett.*, 42, 7148–7155
618 doi:10.1002/2015GL065665, 2015b.
- 619 Lovejoy, S., and Schertzer, D.: Scale invariance in climatological temperatures and the local spectral plateau, *Annales*
620 *Geophysicae*, 4B, 401-410, 1986.,
- 621 Lovejoy, S., and Schertzer, D.: Towards a new synthesis for atmospheric dynamics: space-time cascades, *Atmos. Res.*, 96, 1-52
622 doi:10.1016/j.atmosres.2010.01.004, 2010.
- 623 Lovejoy, S., and Schertzer, D.: Stochastic and scaling climate sensitivities: solar, volcanic and orbital forcings, *Geophys. Res.*
624 *Lett.*, 39, L11702, doi:10.1029/2012GL051871, 2012a.,

- 625 Lovejoy, S., and Schertzer, D.: Low frequency weather and the emergence of the Climate, in *Extreme Events and*
626 *Natural Hazards: The Complexity Perspective*, edited by A. S. Sharma, A. Bunde, D. N. Baker and V. P. Dimri, pp. 231-
627 254, AGU monographs, Washington D.C., 2012b,
- 628 Lovejoy, S., and Schertzer, D.: ,Haar wavelets, fluctuations and structure functions: convenient choices for geophysics,
629 *Nonlinear Proc. Geophys.*, 19, 1-14, doi:10.5194/npg-19-1-2012, 2012c.
- 630 Lovejoy, S., and Schertzer, D.: *The Weather and Climate: Emergent Laws and Multifractal Cascades*, 496 pp., Cambridge
631 University Press, Cambridge, 2013.
- 632 Lovejoy, S., Schertzer, D., and Varon, D.: Do GCM's predict the climate.... or macroweather?, *Earth Syst. Dynam.* , 4, 1–16
633 doi:10.5194/esd-4-1-2013, 2013.,
- 634 Lovejoy, S., Muller, J. P., and Boisvert, J. P.: On Mars too, expect macroweather, *Geophys. Res. Lett.*, 41, 7694-7700,
635 doi:10.1002/2014GL061861, 2014.
- 636 Lovejoy, S., del Rio Amador, L., and Hébert, R.: The ScaLIing Macroweather Model (SLIMM): using scaling to forecast global-
637 scale macroweather from months to Decades, *Earth Syst. Dynam.*, 6, 1–22, doi:10.5194/esd-6-1-2015, 2015.
- 638 Mandelbrot, B. B.: Intermittent turbulence in self-similar cascades: divergence of high moments and dimension of the carrier,
639 *Journal of Fluid Mechanics*, 62, 331-350, 1974.
- 640 Mann, M. E., Cane, M. A., Zebiak, S. E., and Clement, A.: Volcanic and solar forcing of the tropical pacific over the past 1000
641 years, *J. Clim.*, 18, 447-456, 2005.
- 642 Marzban, C., Wang, R., Kong, F., and Leyton, S.: On the effect of correlations on rank histograms: reliability of temperature and
643 wind speed forecasts from fine scale ensemble reforecasts, *Mon. Weather Rev.*, 139, 295–310,
644 doi:doi:10.1175/2010MWR3129.1, 2011.
- 645 Meehl, G. A., Washington, W. M., Ammann, C. M., Arblaster, J. M., Wigley, T. M. L., and Tebaldi, C.: Combinations Of
646 Natural and Anthropogenic Forcings In Twentieth-Century Climate, *J. of Clim.* , 17, 3721-3727, 2004.
- 647 Miller, G. H., Geirsdóttir, Á., Zhong, Y., Larsen, D. J., Otto Bliesner, B. L., Holland, M. M., and Anderson, C.: Abrupt onset of
648 the Little Ice Age triggered by volcanism and sustained by sea-ice/ocean feedbacks, *Geophys. Res. Lett.*, 39, L02708
649 doi:10.1029/2011GL050168, 2012.
- 650 Minnis, P., Harrison, E. F., Stowe, L. L., Gibson, G. G., Denn, F. M., Doelling, D. R., and Smith Jr, W. L.: Radiative Climate
651 Forcing by the Mount Pinatubo Eruption, *Science*, 259 (5100), 1411-1415, 1993.
- 652 Moberg, A., Sonnechkin, D. M., Holmgren, K., Datsenko, N. M., and Karlén, W.: Highly variable Northern Hemisphere
653 temperatures reconstructed from low- and high - resolution proxy data, *Nature*, 433(7026), 613-617, 2005.
- 654 Newman, M.: An Empirical Benchmark for Decadal Forecasts of Global Surface Temperature Anomalies, *J. of Clim.*, 26, 5260-
655 5269, doi:10.1175/JCLI-D-12-00590.1, 2013.
- 656 Newman, M. P., Sardeshmukh, P. D., and Whitaker, J. S.: A study of subseasonal predictability, *Mon. Wea. Rev.*, 131, 1715-
657 1732, 2003.
- 658 Nicolis, C.: Transient climatic response to increasing CO2 concentration: some dynamical scenarios, *Tellus A*, 40A, 50-60,
659 doi:10.1111/j.1600-0870.1988.tb00330.x, 1988.
- 660 Østvand, L., Nilsen, T., Rypdal, K., Divine, D., and Rypdal, M.: Long-range memory in millennium-long ESM and AOGCM
661 experiments, *Earth System Dynamics*, 5, ISSN 2190-4979.s 2295 - 2308.s, doi:10.5194/esd-5-295-2014, 2014.

- 662 Panofsky, H. A., and Van der Hoven, I.: Spectra and cross-spectra of velocity components in the mesometeorological
663 range, *Quarterly J. of the Royal Meteorol. Soc.*, 81, 603-606, 1955.
- 664 Pelletier, J., D.: The power spectral density of atmospheric temperature from scales of 10^2 to 10^6 yr, *EPSL*, 158, 157-164, 1998.
- 665 Peng, C.-K., Buldyrev, S. V., Havlin, S., Simons, M., Stanley, H. E., and Goldberger, A. L.: Mosaic organisation of DNA
666 nucleotides, *Phys. Rev. E*, 49, 1685-1689, 1994.,
- 667 Penland, C., and Sardeshmukh, P. D.: The optimal growth of tropical sea surface temperature anomalies, *J. Climate*, 8, 1999-
668 2024, 1995.
- 669 Pielke, R.: Climate prediction as an initial value problem, *Bull. of the Amer. Meteor. Soc.*, 79, 2743-2746, 1998.
- 670 Ragone, F., Lucarini, V., and Lunkeit, F.: A new framework for climate sensitivity and prediction: a modelling perspective,
671 *Climate Dynamics*, 1-13, 2014.
- 672 Roques, L., Chekroun, M. D., Cristofol, M., Soubeyrand, S., and Ghi, M.: Parameter estimation for energy balance models with
673 memory, *Proc. Roy. Soc. A*, 470 20140349 doi: DOI: 10.1098/rspa.2014.0349, 2014.
- 674 Rybski, D., Bunde, A. Havlin, S., and von Storch, H.: Long-term persistence in climate and the detection problem, *Geophys.*
675 *Resear. Lett.*, 33, L06718-06711-06714, doi:10.1029/2005GL025591, 2006.
- 676 Rypdal, M., and Rypdal, K.: Long-memory effects in linear response models of Earth's temperature and implications for future
677 global warming, *J. Climate*, 27 (14), 5240 - 5258, doi:10.1175/JCLI-D-13-00296.1, 2014.
- 678 Sardeshmukh, P. D., and Sura, P.: Reconciling non-gaussian climate statistics with linear dynamics, *J. of Climate*, 22, 1193-
679 1207, 2009.
- 680 Schertzer, D., and Lovejoy, S.: Physical modeling and Analysis of Rain and Clouds by Anisotropic Scaling of Multiplicative
681 Processes, *Journal of Geophysical Research*, 92, 9693-9714, 1987.
- 682 Schmidt, G. A., et al.: Using paleo-climate model/data comparisons to constrain future projections in CMIP5, *Clim. Past*
683 *Discuss.*, 9, 775-835, doi:10.5194/cpd-9-775-2013, 2013.
- 684 Schmitt, F., Lovejoy, S., and Schertzer, D.: Multifractal analysis of the Greenland Ice-core project climate data., *Geophys. Res.*
685 *Lett*, 22, 1689-1692, 1995.
- 686 Shackleton, N. J., and Imbrie, J.: The $\delta^{18}O$ spectrum of oceanic deep water over a five-decade band, *Climatic Change*, 16, 217-
687 230, 1990.
- 688 Shapiro, A. I., Schmutz, W., Rozanov, E., Schoell, M., Haberreiter, M., Shapiro, A. V., and Nyeki, S.: A new approach to long-
689 term reconstruction of the solar irradiance leads to large historical solar forcing, *Astronomy & Astrophysics*, 529, A67,
690 doi: doi.org/10.1051/0004-6361/201016173, 2011.
- 691 Shindell, D. T., Schmidt, G. A., Miller, R. I., and Mann, M. E.: Volcanic and Solar Forcing of Climate Change during the
692 Preindustrial Era, *J. Clim.*, 16, 4094-4107, 2003.
- 693 Steinhilber, F., Beer, J., and Frohlich, C.: Total solar irradiance during the Holocene, *Geophys. Res. Lett.*, 36, L19704,
694 doi:10.1029/2009GL040142, 2009.
- 695 Van der Hoven, I.: Power spectrum of horizontal wind speed in the frequency range from 0.0007 to 900 cycles per hour, *Journal*
696 *of Meteorology*, 14, 160-164, 1957.
- 697 Varotsos, C., Cartalis, C., Vlamakis, A. Tzani, C. and Keramitsoglou, I.: The long-term coupling between column ozone and
698 tropopause properties, *J Climate*, 17(19), 3843-3854, 2004.

- 699 Vyushin, D., Zhidkov, I., Havlin, S., . Bunde, A., and Brenner, S.: Volcanic forcing improves atmosphere-ocean
700 coupled, general circulation model scaling performance. *Geophys. Res. Lett.*, 31, L10206, doi:10.1029/2004GL019499,
701 2004.
- 702 Wang, Y.-M., Lean, J. L., and Sheeley, N. R. J.: Modeling the Sun's magnetic field and irradiance since 1713, *Astrophys J.* ,
703 625, 522–538, 2005.
- 704 Watson, A. J. and Lovelock, J. E.: Biological homeostasis of the global environment: the parable of Daisyworld, *Tellus*, 35B,
705 284-289, 1983.
- 706 Weber, S. L.: A timescale analysis of the Northern Hemisphere temperature response to volcanic and solar forcing, *Climate of*
707 *the Past*, 1, 9–17, 2005.
- 708 Zanchettin, D., Rubino, A., and Jungclaus, J. H.: Intermittent multidecadal-to-centennial fluctuations dominate global
709 temperature evolution over the last millennium, *Geophys. Res. Lett.*, 37 (14), L14702, 2010.
- 710 Zanchettin, D., Rubino, A., Matei, D., Bothe, O., and Jungclaus, J. H.: Multidecadal-to-centennial SST variability in the MPI-
711 ESM simulation ensemble for the last millennium, *Climate Dynamics*, 40 (5-6), 1301-1318, 2013.
- 712 Zebiak, S. E., and Cane, M. A.: A Model El Niño – Southern Oscillation, *Mon. Wea. Rev.*, 115, 2262–2278, 1987.
713 [http://dx.doi.org/10.1175/1520-0493\(1987\)115%3C2262:AMENO%3E2.0.CO;2](http://dx.doi.org/10.1175/1520-0493(1987)115%3C2262:AMENO%3E2.0.CO;2).
- 714 Zhu, X., Fraederich, L., and Blender, R.: Variability regimes of simulated Atlantic MOC, *Geophys. Res. Lett.*, 33, L21603,
715 doi:10.1029/2006GL027291, 2006.
- 716
- 717

718

Tables:

719

Table 1. The scaling exponent estimates for the forcings and ZC model responses.

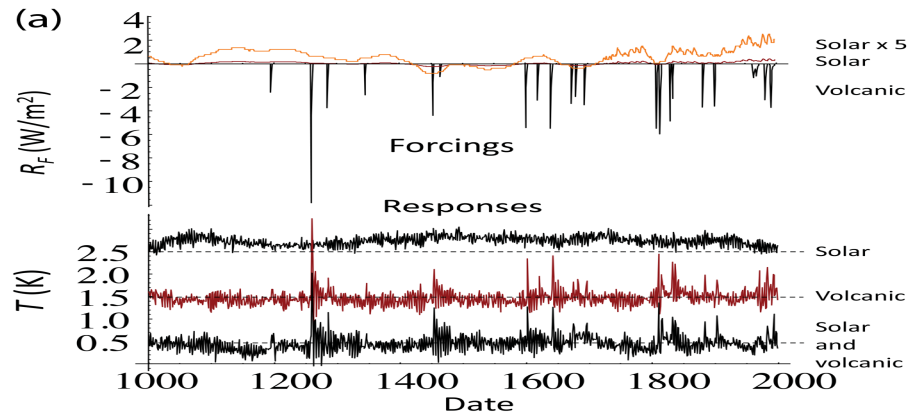
	Forcings		Responses			Control Runs	
	Solar	Volcanic	Solar	Volcanic	Combined	GISS	ECHAM5
H	0.40	-0.21	0.031	-0.17	-0.15	-0.26	-0.4
C_1	0.095	0.48	0.022	0.054	0.038	<0.01	<0.01
α	1.04	0.31	1.82	2.0	2.0	–	–
$\xi(2)/2$	0.33	-0.47	-0.01	-0.28	-0.23	<0.01	<0.01
β	1.66	0.06	0.98	0.44	0.54	0.47	0.2
τ_{eff}	630 yrs	300yrs	100yrs	100 yrs	250 yrs	–	–

720

721 Table 1 shows the scaling exponent estimates for the forcings and ZC model responses. For the solar (forcing and response), only
722 the recent 400 yrs (sunspot based) series were used, for the others, the entire 1000 yrs range was used, see figure 6a. The RMS
723 exponent was estimated from Eq. (6), (9): H was estimated from the Haar fluctuations, α , c_1 were estimated from the trace
724 moments (Fig. 6a). Note that the external cascade scales are unreliable since they were estimated from a single realization. The
725 control runs at the right are for the GISS-E2-R model discussed in the text and (ECHAM5) from the fully coupled COSMOS-
726 ASOB Millenium long term simulations based on the Hamburg ECHAM5 model for 800–4000AD.

727
728

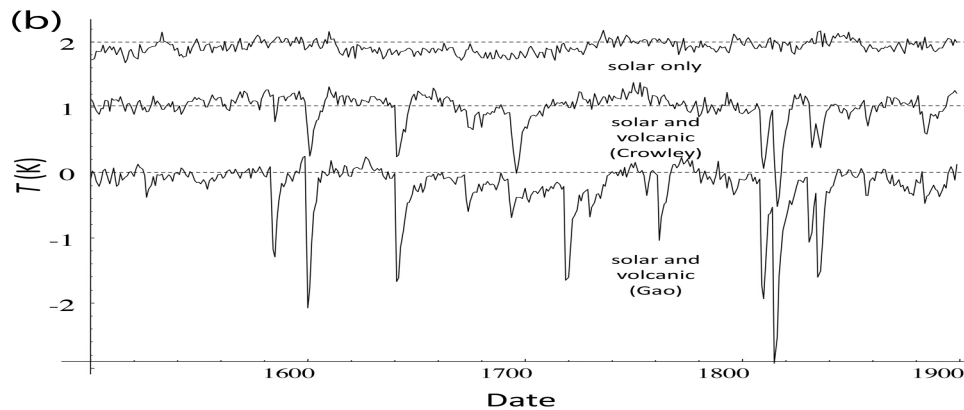
Figures and Captions:



729

730 Figure 1a. Top graph: The radiative forcings R_F (top, W/m^2) and responses T (K) from 1000-2000 AD for the Zebiak–Cane
 731 model, from Mann et al., (2005), integrated over the entire simulation region. The forcings are reconstructed solar (brown), solar
 732 blown up by a factor 5 (orange) and volcanic (red). For the solar forcing (top series), note the higher resolution and wandering
 733 character for the recent centuries – this part is based on sunspots, not ^{10}Be .

734 Bottom graph: The responses are for the solar forcing only (top), volcanic forcing only (middle) and both (bottom); they have
 735 been offset in the vertical for clarity by 2.5, 1.5, 0.5K respectively.

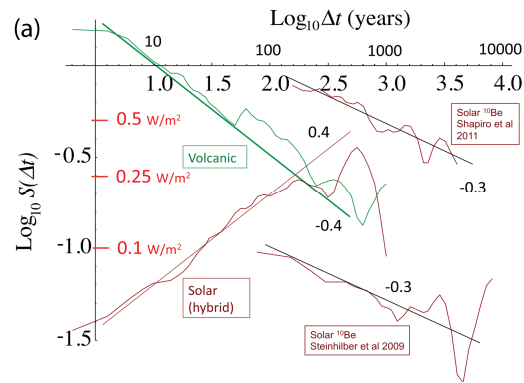


736

737 Figure 1b. GISS-ER-2 responses averaged over land, the northern hemisphere at annual resolution. The industrial part since 1900
 738 was excluded due to the dominance of the anthropogenic forcings. The solar forcing is the same as for the ZC model, it is mostly
 739 sunspot based (since 1610). The top row is for the solar forcing only, the middle series is the response to the solar and Crowley
 740 reconstructed volcanic forcing series (i.e. the same as used in the ZC model); the bottom series uses the solar and reconstructed
 741 volcanic forcing series from Gao et al., (2008). Each series has been offset in the vertical by 1K for clarity (these are anomalies
 742 so that the absolute temperature values are unimportant).

743

744

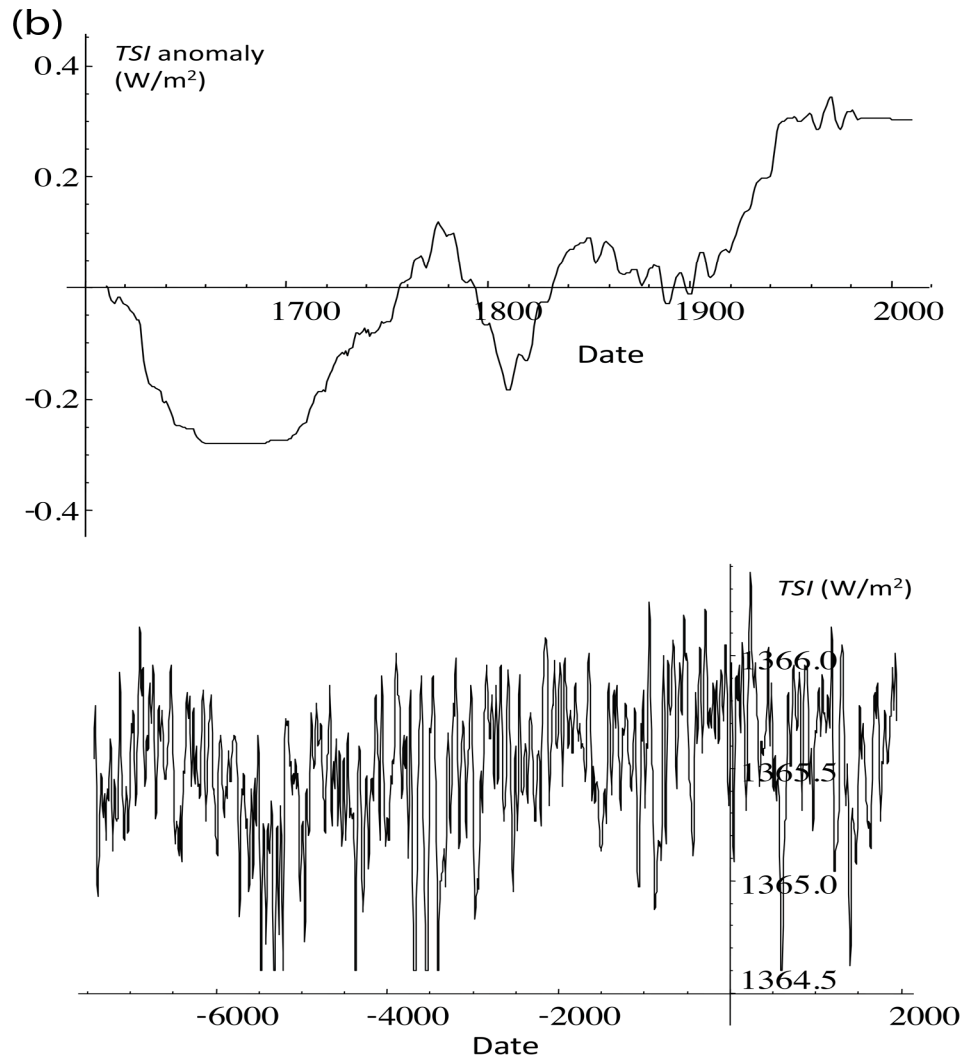


745

746 Figure 2a. The RMS Haar fluctuation $S(\Delta t)$ for the solar and volcanic reconstructions used in the ZC simulation for lags Δt from
 747 2 to 1000 years (left). The solar is a “hybrid” obtained by “splicing” the sunspot-based reconstruction (Fig. 2b, top) with a ^{10}Be
 748 based reconstruction (Fig. 2b, bottom). The two rightmost curves are for two different ^{10}Be reconstructions (Shapiro et al., 2011;
 749 Steinhilber et al., 2009). Although at any given scale, their different assumptions lead to amplitudes differing by nearly a factor
 750 of 10, their exponents are virtually identical and the amplitudes diminish rapidly with scale.

751

752

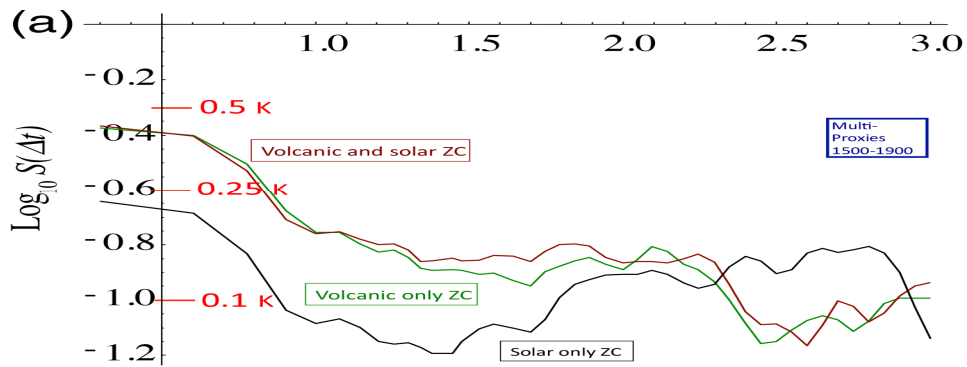


753

754 Figure 2b. A comparison of the sunspot derived Total Solar Irradiance (TSI) anomaly (top, used in the ZC and GISS simulations
 755 back to 1610, $H \approx 0.4$) with a recent ^{10}Be reconstruction (bottom, total TSI - mean plus anomaly - since 7362 BC, see Fig. 2a for a
 756 fluctuation analysis, $H \approx -0.3$) similar to that “spliced” onto the sunspot reconstruction for the period 1000-1610. We can see
 757 that the statistical characteristics are totally different with the sunspot variations “wandering” ($H > 0$) whereas the ^{10}Be
 758 reconstruction is “cancelling” ($H < 0$). The sunspot data were for the “background” (i.e. with no 11 year cycle, see Wang et al.,
 759 2005 for details), the data for the ^{10}Be curve were from Shapiro et al., (2011).

760

761



762

763

764

765

766

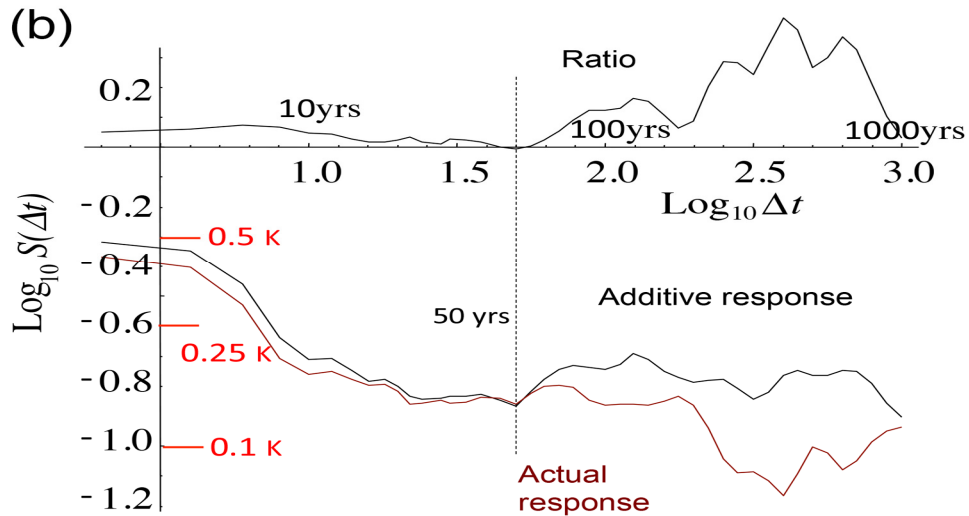
767

768

769

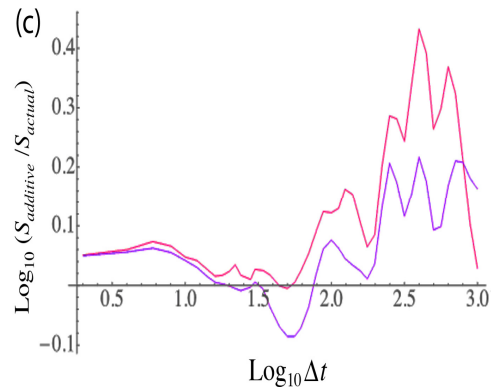
770

Figure 3a. The RMS Haar fluctuations of the Zebiak–Cane (ZC) model responses (from an ensemble of 100 realizations) with volcanic only (green, from the updated Crowley reconstruction), solar only (black, using the sunspot based background (Wang et al., 2005), and both (brown). No anthropogenic effects were modelled. Also shown for reference are the fluctuations for three multiproxy series (blue, dashed, from 1500-1900, pre-industrial, the fluctuations statistics from the three series were averaged, this curve was taken from Lovejoy and Schertzer, 2012b). We see that all the combined volcanic and solar response of the model reproduces the statistics until scales of ≈ 50 -100 years; however at longer time scales, the model fluctuations are substantially too weak – roughly 0.1K (corresponding to ± 0.05 K) and constant or falling, whereas at 400 yr scales, the temperature fluctuations are ≈ 0.25 K (± 0.125) and rising.



771

772 Figure 3b. A comparison of the RMS fluctuations of the ZC model response to combined solar and volcanic forcings (brown,
 773 bottom, from Fig. 3a), with the theoretical additive responses (black, bottom) as well as their ratio ($S_{additive} / S_{actual}$ black, top). The
 774 additive response was determined from the root mean square of the solar only and volcanic only response variances (from Fig.
 775 3a): additivity implies that the fluctuation variances add (assuming that the solar and volcanic forcings are statistically
 776 independent). We can see that after about 50 years, there are strong negative feedbacks, the solar and volcanic forcings are
 777 subadditive, see Fig. 3c for a blow up of the ratio.

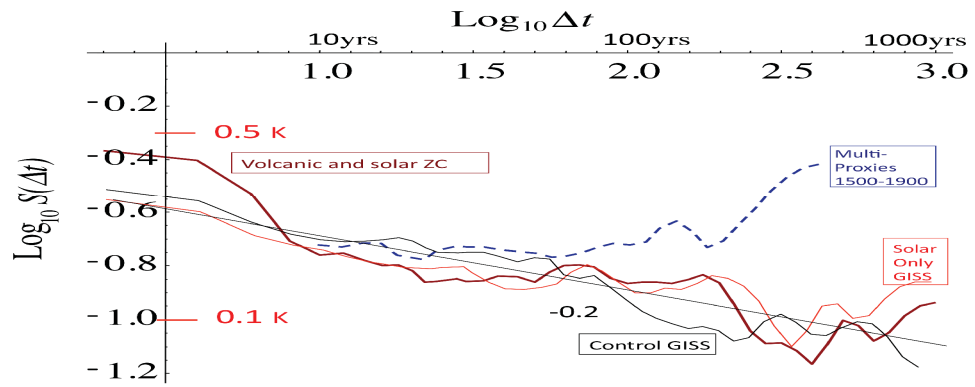


778

779 Figure 3c. An enlarged view of the ratio of the linear to nonlinear responses (from Fig. 3b). The top (magenta) curve assumes
 780 independence of the solar and volcanic forcings, the bottom purple curve uses the actual response to the combined forcings. The
 781 maximum at around 400 yrs (top curve) corresponds to a factor ≈ 2.5 (≈ 1.6 , bottom curve) of negative feedback between the
 782 solar and volcanic forcings. The decline at longer durations (Δt 's the single 1000 yr fluctuation) is likely to be an artefact of the
 783 limited statistics at these scales.

784

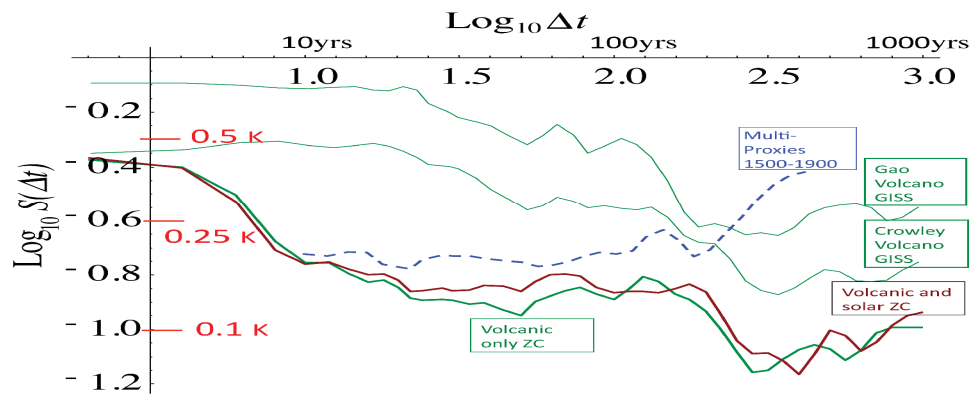
785



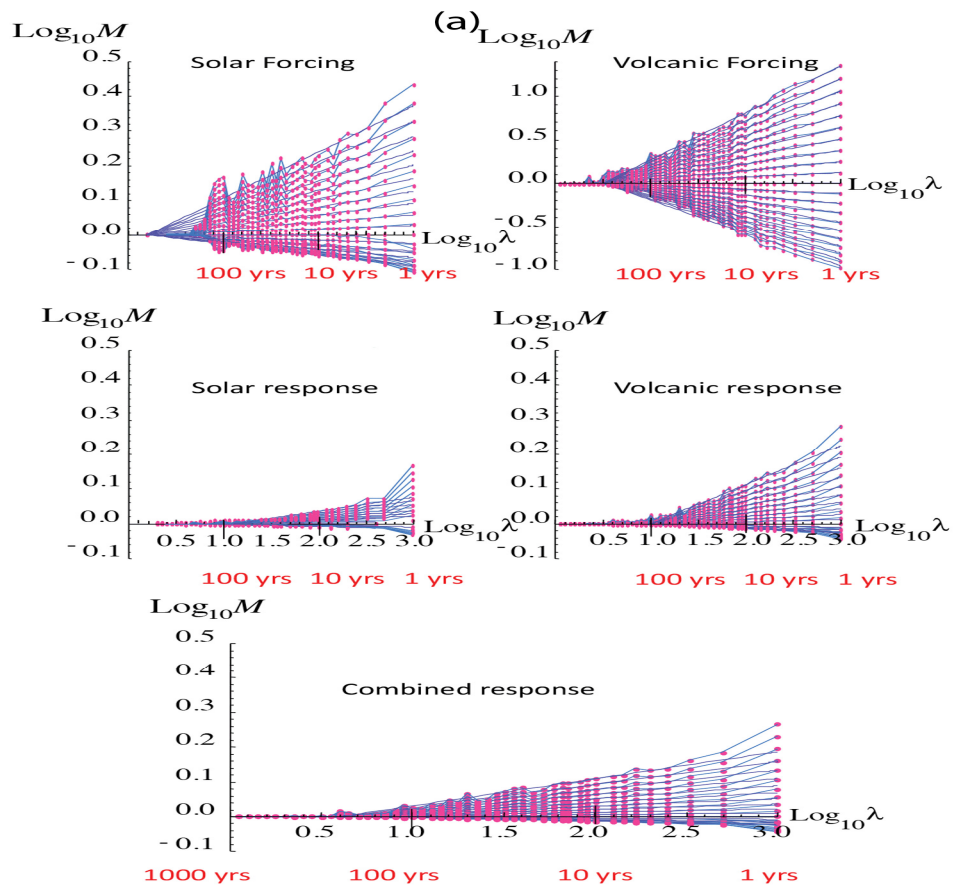
786

787

788 Figure 4. A comparison of the Zebiak-Cane (ZC) model combined (volcanic and solar forcing) response (thick brown) with
 789 GISS-E2-R simulations with solar only forcing (red) and a control run (no forcings, black), the GISS structure functions are for
 790 land, northern hemisphere, reproduced from Lovejoy et al., (2013).



795 Figure 5. A comparison of the volcanic forcings for the ZC model (bottom green) and for the GISS-E2-R GCM for two different
 796 volcanic reconstructions (Gao et al., 2008, and Crowley, 2000) (top green curves, reproduced from Lovejoy et al., 2013). Also
 797 shown is the combined response (ZC, brown) and the preindustrial multiproxies (dashed blue).

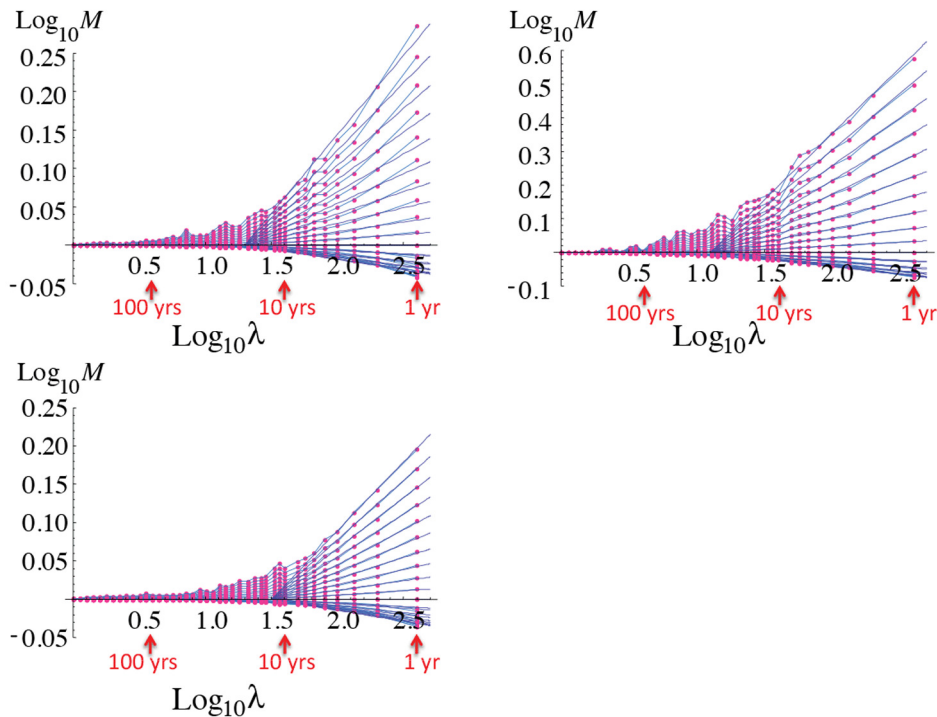


798

799 Figure 6a. Analysis of the fluxes/cascade structures of the ZC forcings (top row) and ZC temperature responses (middle, bottom
800 rows); the normalized trace moments (Eq. (11)) are plotted for $q = 2, 1.9, 1.8, 1.7, 1.6, \dots, 0.1$. Upper left is solar forcing (last 400
801 yrs only, mostly sunspot based), upper right is volcanic, middle left, solar response (last 400 yrs), middle right (volcanic
802 response), lower left, response to combined forcings (last 1000 yrs). Note that all axes are the same except for volcanic. For the
803 solar, only the last 400 yrs were used since this was reconstructed using the more reliable sunspot based method. The earlier ^{10}Be
804 based reconstruction had relatively poor resolution and is not shown. Since the volcanic variability was so dominant, for the
805 combined response (bottom left) the entire series was used. The red points and lines are the empirical values, the blue lines are
806 regressions constrained to go through a single outer scale point. In comparing the different parts of the figure, note in particular i)
807 the log-log linearity for different statistical moments, ii) the fact that the lines for different moments reasonably cross at a single
808 outer scale, and iii) the overall amplitude of the fluctuations – for example by visually comparing the range of the $q = 2$ moments
809 (the top series) as we move from one graph to another.

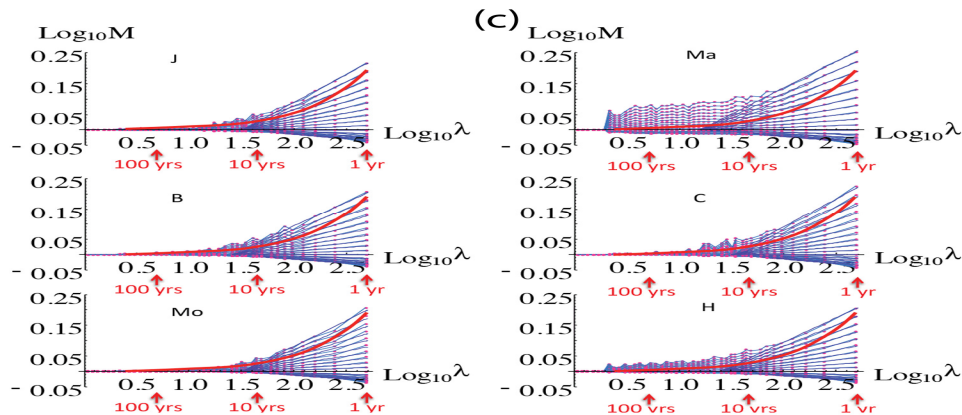
810

(b)



811

812 Figure 6b. The above shows the responses for the GISS-E2-R simulations (northern hemisphere, land, 1500-1900), $\lambda=1$
 813 corresponds to 400 yrs. The upper left is for the response to the Crowley reconstructed volcanic forcings (same as used in the ZC
 814 simulations, not the change in the vertical scale), the upper right for the Gao reconstructed volcanic forcings and the lower left is
 815 for the solar only (mostly sunspot based, same as used in the ZC simulations).



816

817 Figure 6c. Trace moment analysis of six annual resolution multiproxies, J = Jones, Ma = Mann 98, B = Briffa, C = Crowley, Mo
 818 = Moberg, H = Huang, the curves are reproduced with permission from figure 11.8, of Lovejoy and Schertzer, (2013), where full
 819 details and references are given. All were for the pre-industrial period 1500-1900 AD; $\lambda=1$ corresponds to 400 yrs. The curve
 820 shows the generic convergence of the envelope of curves to a quasi-Gaussian process, the proximity of the curve to the envelope
 821 indicates that with the possible exception of the Mann curve, the intermittency is low.

822